Published in final edited form as:
Prog Nucl Magn Reson Spectrosc. 2011 May ; 58(3-4): 176–201. doi:10.1016/j.pnmrs.2010.10.003.

Chemical shift tensors: Theory and application to molecular structural problems

Julio C. Facelli
Department of Biomedical Informatics, Center for High Performance Computing, University of Utah, 155 South 1452 East RM 405, Salt Lake City, UT 84112-0190, United States

Julio C. Facelli: julio.facelli@utah.edu

Keywords

NMR chemical shifts; NMR shielding; Molecular structure

1. The chemical shift tensor

Perhaps the most important discovery after the successful detection of the NMR signal was the observation that nuclear resonance frequencies depend on the chemical or electronic environment of the nuclei [1,2], or as Ramsey states in his landmark papers [3,4] of 1950: "*In measurements of nuclear magnetic moments, a correction must be made for the magnetic field arising from the motions of the molecular electrons which are induced by the externally applied field*." Ramsey realized that corrections using only Lamb's diamagnetic theory were inadequate for molecules, because in molecules there are additional shielding contributions arising from the second order paramagnetism. To address this problem he developed the necessary theoretical framework to explain and eventually to calculate the "chemical effect", which would become the chemical shift commonly used now for structural elucidation. The calculation of the second order paramagnetic contribution to the shielding using perturbation theory has been a challenge to theoreticians for more than fifty years. The progress in this field is reported annually by Jameson and de Dios in the Annual Reviews in NMR Spectroscopy Series [5]. The complete list of review articles published in the literature is not listed here, but for reference purposes we may note recently published reviews and books on the subject [6–9].

The formal properties of the magnetic shielding are discussed below, but it is important to understand that while many scientists think about the chemical shift or magnetic shielding as a number associated with each resonant nucleus, in reality the shielding is a tensor quantity. This means that the screening of the external magnetic field by the electron density of the molecule depends on the relative orientation of the external magnetic field and the molecule; therefore, the shielding phenomena has to be described by a tensor instead of a scalar number. This can be easily observed when recording the NMR spectra of solids. For single crystal samples, where the relative orientation of the molecules with respect to the external magnetic field can be macroscopically controlled by changing the orientation of the crystal with respect to the external field, the orientation dependence can be observed in the change of the position of the resonance lines of the NMR spectra as the crystal is rotated around the magnetic field. In Fig. 1, we present an example of this behavior showing the large differences in the ^{13}C NMR spectra of a single crystal spectra of 1,3,5-trihydroxybenzene at different orientations.

While studies on single crystals provide complete information of the chemical shift tensor, these experiments are quite cumbersome and have been performed on a very limited number

of compounds. Nevertheless the collection of single crystal measurements in sugars and polycyclic aromatic compounds measured by Grant and co-workers at Utah remain one of the most comprehensive and precise benchmark data for shielding calculations in solids [10–21]. Most of the NMR studies [22] are performed on disordered samples where the dependence of the shielding with respect to the orientation of the external magnetic field results in the characteristic powder patterns for solids and narrow single lines for liquids, shown in Fig. 2. The powder patterns originate in the superposition of resonances corresponding to molecules randomly orientated in the sample while the narrow lines are a consequence of the rapid motional averaging in the liquid phase. A complete description of these spectra and how to extract the chemical shift information from them can be found in Ref. [22]. For samples in liquids only the isotropic value of the tensor can be measured. For disordered samples it is possible to obtain the principal components of the tensor; however, except for the cylindrically symmetric case, top spectra in Fig. 2, these patterns do not provide any information on the orientation of the principal axis of the shielding tensor in the molecular frame, which has to be inferred using other methods. Calculations of the shielding tensors have become the most common method for this determination.

There is a considerable lack of consistency in the literature about the use of the terms “chemical shift” and “shielding.” The shielding or more properly the magnetic shielding is the tensor that describes the relative change in the local magnetic field at the nucleus position relative to the external magnetic field. This change in the local magnetic field, which originates in the interaction of the electron cloud with the external magnetic field, can produce shielding or de-shielding of the nucleus. In the first case the local magnetic field is increased with respect to the external field, while in the second case the local field is decreased. In general, shielding effects are associated with diamagnetic effects from spherical charge distributions, while de-shielding effects are associated with a non-spherical charge distribution originating from *p* or higher angular momentum electrons. When experiments are performed at a constant magnetic field, as it is normally done in modern NMR spectrometers, a shielding effect results in a shift of the resonance to a higher frequency, while a de-shielding effect will result in a lower resonance frequency. For historic reasons associated with the early use of fix-frequency/variable field spectrometers, it is still common practice today to associate shielding with the term “up-field shift” and de-shielding with “down-field shift.” New IUPAC (International Union of Pure and Applied Chemistry) recommendations for reporting chemical shifts and magnetic shielding have been published recently by Harris et al. [24].

In practice, NMR experiments do not measure the shielding directly, instead the common practice is to measure the chemical shifts as the change of resonance frequency of a nucleus relative to a given standard. Moreover, for historic reasons it is customary to reverse the frequency scale, i.e. nuclei more shielded than the standard are considered to have positive chemical shifts and those less shielded negative ones.

The formal relation between the chemical shift and shielding tensors is given by:

$$\boldsymbol{\delta} = \mathbf{1}\sigma_{\mathrm{iso}} - \boldsymbol{\sigma}, \quad (1)$$

where $\boldsymbol{\delta}$ is the chemical shift tensor, $\boldsymbol{\sigma}$ is the shielding tensor, $\mathbf{1}$ is the unit matrix and σ_{iso} is the isotropic value or trace of the shielding tensor of the standard reference used in the NMR experiments. The determination of the values of σ_{iso}, usually known as absolute chemical shift, is quite difficult and involves the determination of the paramagnetic contribution to the shielding using its relationship with the spin rotational constant and the calculation of the corresponding diamagnetic part using quantum mechanical methods [25]. The procedure for selecting primary and secondary reference compounds has been discussed extensively by

Jameson and Mason in Chapter 3 of Ref. [26]. The absolute shielding values have to be corrected for vibrational averaging, bulk magnetic susceptibility, temperature, etc. and later related to secondary standards that can be easily used in NMR measurements. Some examples of absolute shieldings for commonly used reference compounds are given in Table 1.

1.1. Symmetry properties of the shielding tensor

The formal definition of the components of the shielding tensor is:

$$\sigma_{\alpha\beta}=\frac{\partial^2 E}{\partial \boldsymbol{\mu}_\alpha \partial \mathbf{B}_\beta}, \quad (2)$$

where E is the total electronic energy of the molecule; **B** is the external magnetic field and **μ** is the magnetic moment of the nucleus of interest. There are two important observations that can be made from Eq. (2).

i. The shielding tensor is an antisymmetric tensor because exchanging the sub indices α and β in Eq. (2) leads to a different quantity. Note that this permutation exchanges the components of the magnetic moment **μ** and magnetic field **B**, with respect to which the derivative of the energy is calculated, i.e.

$$\sigma_{\alpha\beta}=\frac{\partial^2 E}{\partial \boldsymbol{\mu}_\alpha \partial \mathbf{B}_\beta}=\frac{\partial^2 E}{\partial \mathbf{B}_\beta \partial \boldsymbol{\mu}_\alpha} \neq \frac{\partial^2 E}{\partial \boldsymbol{\mu}_\beta \partial \mathbf{B}_\alpha}=\sigma_{\beta\alpha}. \quad (3)$$

This property of the tensor should not to be confused with the fact that the first order response function to the shielding interaction, i.e. the NMR spectrum, is sensitive only to the symmetric part of the tensor and that the antisymmetric components contribute only to the second order response, i.e. the relaxation of the spin magnetization [27–29].

ii. When using perturbation theory for the expansion of the molecular energy in powers of the external magnetic field and the nuclear magnetic moment, the shielding tensor components can be identified as the coefficients in the expansion that are bilinear terms in the nuclear magnetic moment and the external magnetic field.

The shielding tensor, when expressed in an arbitrary Cartesian frame, *x, y, z*, fixed to the molecule has nine independent components. This number may be reduced by choosing a reference system that reflects the symmetry of the molecule. The independent components of the shielding tensor for different point group symmetries at the nucleus under consideration are given in Table 2 [30]. Note that the diamagnetic contribution to the shielding tensor is a symmetric quantity, a fact that will become apparent when we develop the perturbation expansions for the shielding tensors.

2. Theory of the magnetic shielding tensor

To obtain exact expressions for the calculation of shieldings using the non-relativistic Born–Oppenheimer approximation, it is necessary to include the vector potential representing the external magnetic field and the dipolar field from the magnetic moment of the nucleus in the electronic Hamiltonian [31]. In electromagnetic theory the magnetic field is included in the Hamiltonian as the curl of the vector potential **A**. This vector potential is not unique, because the addition of the gradient of any continuously differentiable scalar function produces the same magnetic field. This follows from the fact that the curl of the gradient is

zero. This no uniqueness leads to a degree of freedom in the formulation of electrodynamics, or gauge freedom, and requires choosing a gauge. In the gauge of Coulomb [31] the vector potential defining these fields at the position of the electron k can be written as:

$$\mathbf{A}_k(\mathbf{r})=\frac{1}{2}\mathbf{B}\times\mathbf{r}_k+(\boldsymbol{\mu}_N\times\mathbf{r}_{Nk})/\mathbf{r}_{Nk}^3, \quad (4)$$

where the standard notation is used, the origin of the vector potential is at the position **O** and $\mathbf{r}_k$ and $\mathbf{r}_{Nk}$ are defined according to Fig. 3. Note that for simplicity we are considering that only one nucleus in the molecule has a non-zero magnetic moment.

Following the standard procedures for the inclusion of magnetic interactions into the electronic Hamiltonian [31], the full electronic Hamiltonian in the presence of the external and dipolar magnetic fields becomes:

$$H=\frac{1}{2}\sum_k\left[\frac{1}{i}\nabla_k-\frac{1}{c}\mathbf{A}_k(\mathbf{r})\right]^2+\mathbf{V}(\mathbf{r}_k), \quad (5)$$

where $\mathbf{V}(\mathbf{r})$ is the scalar potential, which in the case of molecules include all the Columbic integrations between the electrons and the nuclei and $\mathbf{r}$ is the position of the k electron from an arbitrary origin. Using the properties of the gauge of Coulomb, i.e. $\nabla\cdot\mathbf{A}=0$, the expansion of this Hamiltonian beyond zero order leads to six terms of which only three are relevant to the calculation of shieldings. These terms are:

$$H_\alpha^{(1,0)}=\frac{-i}{2c}\sum_k L_{k_\alpha}=\frac{-i}{2c}\sum_k(\mathbf{r}_k\times\nabla_k)_\alpha, \quad (6)$$

$$H_\alpha^{(0,1)}=\frac{-i}{c}\sum_k\frac{L_{Nk_\alpha}}{\mathbf{r}_{Nk}^3}=\frac{-i}{2c}\sum_k\frac{(\mathbf{r}_{Nk}\times\nabla_k)_\alpha}{\mathbf{r}_{Nk}^3}, \quad (7)$$

$$H_{\alpha\beta}^{(1,1)}=\frac{1}{c^2}\sum_k\frac{\left(\mathbf{r}_k\cdot\mathbf{r}_{Nk}\delta_{\alpha\beta}-\mathbf{r}_{k_\alpha}\cdot\mathbf{r}_{Nk_\beta}\right)}{\mathbf{r}_{Nk}^3}, \quad (8)$$

where L_{k_α} and L_{Nk_α} are the angular momentum of the electron k with respect to the origin of coordinates and to the nucleus N, respectively. If we restrict our analysis to closed shell molecules, for which the electronic ground state is of the Σ type, the expansion of the Hamiltonian at order 1 in the magnetic field and nuclear magnetic moment, $H^{(1,0)}$ and $H^{(0,1)}$, respectively have zero contribution to the energy using first order Rayleigh-Schrödinger (RS) perturbation theory. This leaves no other terms of order $1/c$ contributing to the shielding. The third term, $H^{(1,1)}$, gives a non-zero contribution using first order RS perturbation theory that is proportional to $1/c^2$. A second contribution of order $1/c^2$ can be obtained, at second order, from the cross term between $H^{(1,0)}$ and $H^{(0,1)}$. Using the definition of shielding given by Eq. (2), we can identify the diamagnetic and paramagnetic contributions to the shielding as these two first and second order terms in the RS perturbation expansion. The final expressions for the diamagnetic and paramagnetic contributions are given by:

$$\sigma_{\alpha\beta}^d(\mathbf{O})=\frac{1}{2c^2}\left\langle\psi_0\left|\left(\mathbf{r}_k\cdot\mathbf{r}_{Nk}\delta_{\alpha\beta}-\mathbf{r}_{k_\alpha}\cdot\mathbf{r}_{Nk_\beta}\right)\mathbf{r}_{Nk}^{-3}\right|\psi_0\right\rangle, \quad (9)$$

$$\sigma^{p}_{\alpha\beta}(\mathbf{O})=\frac{-1}{2c^2}\sum_{n}\frac{1}{E_n-E_0}\langle\psi_0|L_{k_\alpha}|\psi_n\rangle\langle\psi_n|L_{Nk_\beta}\mathbf{r}^{-3}_{Nk}|\psi_0\rangle+\text{C.C.} \quad (10)$$

We have thus indicated explicitly that Eqs. (9) and (10) are valid when the origin of the vector potential is at the position **O**. The sum in Eq. (10) is over all the exited states of the molecule; however, before discussing methods for practical evaluation of Eqs. (9) and (10) it is important to understand the behavior of the diamagnetic and paramagnetic terms under translation of the coordinate origin. As shown by Eqs. (9) and (10), both terms exhibit an explicit dependence on the origin of coordinates used in the calculations. Using the notation of Fig. 3 we can calculate the effect of a translation of the origin of coordinates on the diamagnetic and paramagnetic contribution by using the following replacements

$$\begin{aligned}\mathbf{r}_{Nk}&=\mathbf{r}'_{Nk},\\ \mathbf{r}_{k}&=\mathbf{r}'_{k}+\mathbf{R}_{\mathbf{O}'}\end{aligned} \quad (11)$$

in Eqs. (9) and (10) to obtain the expressions for $\boldsymbol{\sigma}^{d}$ and $\boldsymbol{\sigma}^{p}$ in the new coordinate system with origin in $\mathbf{O}'$. For the diamagnetic components we obtain:

$$\sigma^{d}_{\alpha\beta}(\mathbf{O})=\frac{1}{2c^2}\left\langle\psi_0\middle|\left(\mathbf{r}'_{k}\cdot\mathbf{r}_{Nk}\delta_{\alpha\beta}+\mathbf{R}_{\mathbf{O}'}\cdot\mathbf{r}_{Nk}\delta_{\alpha\beta}-\mathbf{r}'_{k_\alpha}\cdot\mathbf{r}_{Nk_\beta}-\mathbf{R}_{\mathbf{O}'_\alpha}\cdot\mathbf{r}_{Nk_\beta}\right)\mathbf{r}^{-3}_{NK}|\psi_0\right\rangle \quad (12)$$

which becomes

$$\sigma^{d}_{\alpha\beta.}(\mathbf{O})=\sigma^{d}_{\alpha\beta}(\mathbf{O}')+\frac{\mathbf{R}_{\mathbf{O}'}}{2c^2}\cdot\left\langle\psi_0\left|\frac{\mathbf{r}_{Nk}}{\mathbf{r}^{3}_{NK}}\right|\psi_0\right\rangle\delta_{\alpha\beta}-\mathbf{R}_{\mathbf{O}'_\alpha}\left\langle\psi_0\left|\frac{\mathbf{r}_{Nk_\beta}}{\mathbf{r}^{3}_{NK}}\right|\psi_0\right\rangle. \quad (13)$$

The same replacements can be done for the paramagnetic contribution

$$\sigma^{p}_{\alpha\beta}(\mathbf{O})=\frac{-1}{2c^2}\sum_{n}\frac{1}{E_n-E_0}\langle\psi_0|((\mathbf{r}'_{k}+\mathbf{R}_{\mathbf{O}'})\times\nabla)_\alpha|\psi_n\rangle\left\langle\psi_n|L_{Nk_\beta}\mathbf{r}^{-3}_{Nk}|\psi_0\right\rangle+\text{C.C.} \quad (14)$$

which becomes

$$\sigma^{p}_{\alpha\beta.}(\mathbf{O})=\sigma^{p}_{\alpha\beta}(\mathbf{O}')+\left(\frac{-1}{2c^2}\sum_{n}\frac{1}{E_n-E_0}\langle\psi_0|(\mathbf{R}_{\mathbf{O}'}\times\nabla)_\alpha|\psi_n\rangle\times\left\langle\psi_n\left|(\mathbf{r}_{Nk}\times\nabla_k)_\beta\mathbf{r}^{-3}_{Nk}\right|\psi_0\right\rangle+\text{C.C.}\right). \quad (15)$$

At this point of the derivation it is crucial to assume that we are working with the exact solution of the Schrödinger equation, therefore the $|\psi\rangle$ form a complete set for which the virial relationship:

$$(E_n-E_0)\langle\psi_0|\mathbf{r}|\psi_n\rangle=\langle\psi_0|\nabla|\psi_n\rangle \quad (16)$$

holds exactly. Note that this relationship is also true for any variational solution of the Schrödinger equation in a complete Hilbert space [32], making the shielding calculations gauge invariant for any variational wave function in a complete Hilbert space.

Using Eq. (16) it is possible to eliminate the energy denominator in Eq. (15) as

$$\sigma^{p}_{\alpha\beta}(\mathbf{O})=\sigma^{p}_{\alpha\beta}(\mathbf{O}')+\left(\frac{-1}{2c^2}\sum_{n}(\mathbf{R}_{\mathbf{o}'}\times\langle\psi_0|\mathbf{r}_k|\psi_n\rangle)_{\alpha}\times\left\langle\psi_n\left|(\mathbf{r}_{Nk}\times\nabla_k)_{\beta}\mathbf{r}_{Nk}^{-3}\right|\psi_0\right\rangle+\text{C.C.}\right) \quad (17)$$

using of the closure relationship $\Sigma_n|\psi_n\rangle\langle\psi_n|=1$ and that the commutator $[\mathbf{r},\nabla]=-1$ can be written as:

$$\sigma^{p}_{\alpha\beta.}(\mathbf{O})=\sigma^{p}_{\alpha\beta}(\mathbf{O}')-\frac{\mathbf{R}_{\mathbf{o}'}}{2c^2}\cdot\left\langle\psi_0\left|\frac{\mathbf{r}_{Nk}}{\mathbf{r}_{Nk}^3}\right|\psi_0\right\rangle\delta_{\alpha\beta}+\mathbf{R}_{\mathbf{o}'_{\alpha}}\left\langle\psi_0\left|\frac{\mathbf{r}_{Nk_{\beta}}}{\mathbf{r}_{Nk}^3}\right|\psi_0\right\rangle. \quad (18)$$

There are several important observations that can be derived from Eqs. (13) and (18).

- **i.** The total shielding, i.e. the sum of the paramagnetic and diamagnetic parts, is invariant under changes of the origin of coordinates. Note that all the terms in Eqs. (13) and (18) that depend on $\mathbf{R}_{\mathbf{O}'}$ cancel each other in the sum of the two expressions. In the language of electromagnetic interactions this is equivalent to saying that the shielding tensor is invariant under gauge transformations that preserve $\nabla\cdot\mathbf{A}=0$, i.e within the gauge of Coulomb. For calculations of the shieldings in other gauges the reader can consult the work by Ferraro et al. [33].
- **ii.** The diamagnetic and paramagnetic components depend on the origin of coordinates and their values can be changed at will by changing the relative position of the nucleus with respect to the origin of coordinates. The origin dependent contributions to the diamagnetic and paramagnetic terms are linear in the distance between the nucleus and the origin of coordinates.
- **iii.** For exact wave functions, actually for any variational approximation of the wave function in a complete Hilbert space, the selection of the coordinate origin is inconsequential because the origin dependent terms in the diamagnetic and paramagnetic contributions are calculated exactly and they cancel each other.
- **iv.** For atomic systems there is a natural selection for the origin of the vector potential, the position of the nucleus. For this selection it is straightforward to prove that the paramagnetic contribution is identically zero and therefore the shielding is totally diamagnetic (Lamb's diamagnetic theory).
- **v.** For approximate wave functions, i.e. any calculation that can be done numerically, the selection of the origin of the gauge is a serious problem because the origin dependent terms, which cancel each other in exact calculations, are calculated using different approximations with different errors and they do not cancel each other. Note that the diamagnetic contributions are calculated using the more accurate zero order perturbation theory while the paramagnetic contributions are calculated using second order perturbation, which is much more sensitive to truncation errors in the sum over the exited states. Numerical examples of the effect of changing the gauge origin in shielding calculations abound in the literature [34] and are discussed in Section 4.6.
- **vi.** One particular selection of the origin of the gauge deserves special mention. If one chooses the origin of the vector potential at the center of mass of the molecule it is possible to prove that the paramagnetic contribution at the center of mass is proportional to the spin-rotational constant, which can be measured by microwave spectroscopy [25,35]. By measuring the spin-rotational constant and calculating the diamagnetic contribution to the shielding at the center of mass it is possible to

obtain very accurate determinations of the absolute shieldings of the nuclei in small molecules, which are used to establish absolute shielding scales.

vii. For molecules with C_∞ symmetry where the nuclei has to lie on the C_∞ axis, if we choose the origin of coordinates on the C_∞ axis, the component of the paramagnetic contribution along the axis is identically zero and therefore the shielding along the C_∞ axis is totally diamagnetic [36].

viii. Practical experience as well as theoretical derivations have demonstrated that the best results can be obtained when the gauge origin is located at the center of the electronic distribution of the molecule. This choice produces the best overall selection when the shieldings of all the nuclei in the molecule are computed from one single calculation. When only the shielding of one nucleus is required, the best choice for the origin of the vector potential is the position of the nucleus under consideration.

The theory presented above is correct within the non-relativistic approximation. This is of minor consequence when dealing with molecules including first or second row atoms, but becomes a significant problem when the molecule includes atoms beyond the third row of the periodic table. There is a great deal of literature dealing with relativistic effects on chemical shielding calculations [37–47], but there are no well-established methods that can be used routinely. Moreover, the most common approximations to take into account relativistic effects have not been implemented in the most popular software used for chemical shielding calculations. The calculation of chemical shieldings in molecules containing heavy atoms remains the realm of very specialized research groups, a situation that is changing as a consequence of the implementation of shielding calculation using the ZORA (Zeroth Order Regular Approximation to the Dirac equation) approach [48]. Recent work reporting relativistic calculations can be found in Refs. [48–68].

3. Need for shielding calculations

There are several scientific reasons to pursue research efforts in calculating shieldings; the two most common applications are:

i. Testing of quantum chemical methods.

ii. Finding correlations between measurable properties, i.e. chemical shifts, and molecular structure and environment.

The first motivation has been a driving factor for the calculation of chemical shifts for many years as quantum chemical methods to calculate electronic structure have evolved over the years and new and more powerful ones became available. Because the calculation of the electronic wave function provides little information that can be compared with experimental measurements to evaluate the quality of the predicted electronic structure, considerable effort has been devoted to calculating values from the electronic structure spectroscopic properties that can be compared with available experimental data. The great availability of experimental chemical shift information and its sensitivity to the electronic structure has always prompted great interest in their calculation by computational chemists. Numerous reviews have presented the state of the art in the field over the years and a list of the most recent ones can be found in Refs. [6,8,9,69–78].

The second motivation is a consequence of the strong sensitivity of the chemical shifts to molecular structure [79]. While the relationship between structure and chemical shift is not simple because it is mediated by the complex quantum mechanical machinery presented in the following sections of this review, the correlations are powerful. With the advent of

modern computational methods they have been used to establish the emerging field of NMR crystallography [80–89], which is discussed in Section 8.7 of this review.

The material presented in this paper is restricted to the chemical shifts and shielding calculations in diamagnetic molecules. When the molecular electronic ground state is not a singlet, i.e. there are unpaired electrons present in the sample, additional mechanisms contributing to the shielding are present. A comprehensive discussion of these mechanisms and their calculations is presented in Ref. [90].

4. Algorithms for calculation of shielding tensors

In this section we describe different schemes that can be used in practical calculations of shieldings. To avoid unnecessary complications with the gauge problem discussed above, we will discuss the perturbation schemes assuming that we are using a complete basis set. Schemes to alleviate the gauge problem when using finite basis sets are discussed later in Section 4.6. To simplify our expressions we have chosen the position of the nucleus under consideration as the origin of the vector potential. With these choices the expressions for the diamagnetic and paramagnetic terms become:

$$\sigma^{d}_{\alpha\beta}(\mathbf{N}) = \frac{1}{2c^2}\left\langle \psi_0 \left| \left(\mathbf{r}^2_{Nk}\delta_{\alpha\beta} - \mathbf{r}_{Nk_\alpha} \cdot \mathbf{r}_{Nk_\beta} \right) \mathbf{r}^{-3}_{Nk} \right| \psi_0 \right\rangle, \quad (19)$$

$$\sigma^{p}_{\alpha\beta}(\mathbf{N}) = \frac{-1}{2c^2}\sum_n \frac{1}{E_n - E_0}\langle \psi_0 | L_{k_\alpha} | \psi_n \rangle \langle \psi_n | L_{Nk_\beta} \mathbf{r}^{-3}_{Nk} | \psi_0 \rangle + \text{C.C.} \quad (20)$$

The calculation of the diamagnetic part presents no complications and can be evaluated for any kind of wave function. This only requires the computation of one electron integrals of the type $\langle \psi_0 | 1/r | \psi_0 \rangle$, $\langle \psi_0 | 1/r^3 | \psi_0 \rangle$ and $\langle \psi_0 | xy/r^3 | \psi_0 \rangle$, which are readily available in most quantum chemical codes. Moreover, because the ground electronic state is less sensitive to the approximations used in its calculation it is possible to calculate the diamagnetic contribution with good accuracy, even when using modest approximations to the wave function.

The more complicated paramagnetic term requires, in principle, a knowledge of all the exited electronic states of the molecule, in which case direct evaluation of Eq. (20) is necessary. Unfortunately, the excited state wave functions are not known and a great deal of effort is necessary to obtain reliable values of the paramagnetic contribution. It is always important to calculate the paramagnetic contribution with the same accuracy as the diamagnetic contribution to achieve the greatest possible gauge invariance of the numerical results. However, this may increase the computational complexity beyond practical limits, making the evaluation of the paramagnetic contribution the limiting factor in the calculations of shieldings. Historically, better and better approximations have been feasible due to advances in computational science as well as the development of a better understanding of perturbation theory in many electron systems. In the following subsections, we review the most common approximations used in calculating the paramagnetic contribution to the shielding.

4.1. Semiempirical and empirical calculations

Semiempirical calculations of magnetic shieldings, in which the electronic Hamiltonian and the one and two electron interactions are replaced by parametric formulas, were very popular several years ago [91–93]. However, their use has declined substantially in recent

years [94–96] because they are almost as computationally intensive as DFT (Density Functional Theory) calculations using small basis sets that can produce results of equal or even better quality. For this reason the semiempirical calculations are not discussed in any detail in this review.

On the other hand, the development of fast and accurate methods to calculate ^{13}C and ^{1}H NMR chemical shifts using purely empirical models continues to be a very active area of research because these methods provide extremely fast calculations that are useful for high throughput studies. It is important to realize that the empirical methods are not an approximation of the exact formulation of the shielding; therefore, their predictive value is limited by the chemical shifts and structures used as the training set.

The literature of empirical calculation of chemical shieldings has been reviewed extensively in Refs. [97,98]. A recent application of this empirical methodology can be found in an article that describes a fast and accurate method for the prediction of ^{13}C NMR chemical shifts using a data base containing more than 2 million chemical shifts [99]. The high speed of chemical shift calculations is achieved using a simple structure description scheme based on individual atoms rather than functional groups. The approach provides accuracy comparable with other well known approaches, predicting up to 10,000 ^{13}C chemical shifts per second with a standard deviation of 2.76 ppm. Another popular empirical method is TALOS (Torsion Angle Likeliness Obtained from Shift and Sequence Similarity), a hybrid method for predicting protein backbone torsion angles based on chemical shifts [100–102]. The TALOS approach is based on the observation that the chemical shift in proteins depends strongly on the local structure. The most recent version of this software uses data from 200 proteins and a two layer neural network. It can predict the backbone angles of 88.5% residues with a standard deviation of 5.5% [100].

4.2. Coupled Hartree-Fock perturbation theory

The Hartree-Fock (HF) approximation is the foundation for all the practical methods used to calculate shielding; therefore, we present here a careful derivation of the analytical expressions for the magnetic shielding within the HF approximation. Using the HF approximation and standard notation [103] the second order change in the molecular electronic energy, $E^{(2)}$, for a singlet perturbation H_1 is:

$$E^{(2)}=\sum_{\{i,a\}}\{c_{i,a}^2(\varepsilon_a-\varepsilon_i+\langle ia|ia\rangle)+2c_{i,a}\langle i|H_1|a\rangle\}+2\sum_{i,a\neq j,b}\sum c_{i,a}c_{j,b}\{4\langle ia|jb\rangle-\langle ab|ij\rangle-\langle ja|ib\rangle\}, \quad (21)$$

where $c_{i,a}$ are the coefficients corresponding to the exited state determinants in which we have expanded the perturbed wave function as:

$$|\psi\rangle=|\psi_0\rangle+\sum_{i,a}c_{i,a}|\psi_{i\to a}\rangle+\sum_{\substack{i,a\\j,b}}c_{i,a}c_{j,b}\Big|\psi\ \begin{matrix} i\to a\\ j\to b\end{matrix}\ \rangle+\cdots \quad (22)$$

The derivation of Eqs. (21) and (22) is beyond the scope of this review and interested readers should consult Ref. [103]. The Hartree-Fock solution for the ground state corresponds to the single determinant wave function that minimizes the electronic energy of the system, therefore to be consistent with this definition, we will require that the second order energy, $E^{(2)}$, become also a minimum with respect to changes in the expansion coefficients $c_{i,a}$. Using this condition, $\frac{\partial E^{(2)}}{\partial c_{ia}}=0$ in Eq. (21), we obtain the following system of linear equations to calculate the coefficients $c_{i,a}$

$$c_{i,a}(\varepsilon_a - \varepsilon_i + \langle ia|ia\rangle) + \langle i|H_1|a\rangle + 2\sum_{j,b\neq i,a} c_{j,b}\{4\langle ia|jb\rangle - \langle ab|ij\rangle - \langle ja|ib\rangle\} = 0. \quad (23)$$

The second order Hartree-Fock energy can be calculated by entering the values of the $c_{i,a}$ coefficients determined from this system of linear equations, Eq. (23) into Eq. (21).

Several schemes have been develop to solve exactly or approximately the system of linear equations given by Eq. (23). The simplest approximation is to neglect all of the two electron integrals in Eq. (23), the uncoupled approximation, which leads to a very simple expression for the second order energy given by:

$$E^{(2)} = \sum_{i,a} \frac{\langle i|H_1|a\rangle\langle a|H_1|i\rangle}{\varepsilon_i - \varepsilon_a}, \quad (24)$$

where i and a are the indices referring to occupied and exited states, respectively. Direct use of Eq. (24) is problematic because the Hartree-Fock orbital energies for the unoccupied orbitals, ε_a are always too high. Therefore, even when using uncoupled schemes it is necessary to take into account the repulsion integrals $\langle ia|ia\rangle$ to correct for this deficiency in the orbital energies of the unoccupied orbitals. With this correction Eq. (24) becomes:

$$E^{(2)} = \sum_{i,a} \frac{\langle i|H_1|a\rangle\langle a|H_1|i\rangle}{\varepsilon_i - \varepsilon_a + \langle ia|ia\rangle}. \quad (25)$$

The practical application of Eq. (25) to the calculation of the paramagnetic contribution of the shielding can be accomplished by replacing H_1 by the appropriate operators given by Eqs. (6) and (7) and by expanding the molecular orbitals, $|i\rangle$, in a linear combination of atomic orbitals. In general the uncoupled approaches have been less than successful, but many semiempirical theories of the shieldings have been developed by further simplication of Eq. (25). These semiempirical theories assume than only the first term in Eq. (25) makes a significant contribution to the shielding and that the excitation energies in the denominator can be replaced by an average value. Therefore, the sum over the exited states in Eq. (25) is replaced by a quantity solely dependent of the electronic ground state in the numerator divided by the average excitation energy. These two quantities are usually treated as semiempirical parameters fitted to experimental data. By eliminating the sum over states these empirical theories provide very compact expressions for the semi qualitative analysis of the shieldings [104] but they have relative low predictive capabilities.

The next step in complexity for the calculation of the shielding is to solve the system of Eq. (23) including all of coupling terms. This takes into account the change in the average Hartree-Fock potential induced by the external perturbation and the consequent change in the electronic distribution. This physical interpretation has been used as a reason for solving the system of Eq. (23) in an iterative fashion, solving first the uncoupled problem, using its solution to calculate the correction terms in Eq. (23) and iterating thereafter until convergence. This procedure is commonly named Coupled Hartree-Fock (CHF) and its working equations are given by:

$$c_{i,a}^{(n+1)} = \frac{-\langle i|H_1|a\rangle}{\varepsilon_a - \varepsilon_i} - \frac{1}{\varepsilon_a - \varepsilon_i}\sum_{j,b} S_{ia,jb} c_{j,b}^{(n)}, \quad (26)$$

where n indicates the order of the iteration and $S_{ia,jb}$ is given by:

$$S_{ia,jb}=4\langle ia|jb\rangle-\langle ab|ij\rangle-\langle ja|ib\rangle. \quad (27)$$

Note that $S_{ia,jb}$ is independent of the perturbation and depends only on the properties of the Hartree-Fock electronic ground state. The iterative procedure prescribed by Eq. (26) converges if all the eigenvalues of $S_{ia,jb}$ are <1 in absolute value. In contrast with the serious problems encountered in solving these equations for the calculation of J couplings [105], the convergence of the CHF equations for shielding calculations is usually satisfactory.

It is also possible to express the CHF equations in the language of the polarization propagator approach or linear response theory by introducing the inverse of the polarization propagator, **P**,

$$\mathbf{P}^{-1}_{ia,jb}=(\varepsilon_a-\varepsilon_i)\delta_{ij}\delta_{ab}+4\langle ia|jb\rangle-\langle ab|ij\rangle-\langle ja|ib\rangle. \quad (28)$$

Using the definition of $\mathbf{P}^{-1}$ in Eq. (28) it is possible to express the second-order contribution to the electronic energy as:

$$E^{(2)}=\sum_{\substack{ia\\jb}}\langle i|H_1|a\rangle\mathbf{P}_{ia,jb}\langle b|H_1|j\rangle. \quad (29)$$

There are several relevant features of Eq. (29) that are important to discuss.

- **i.** The propagator **P** depends only on quantities which are known from the Hartree-Fock calculations (see Eq. (28)).
- **ii.** Once the polarization propagator **P** has been calculated by inverting $\mathbf{P}^{-1}$, it is possible to calculate any second-order property depending on it by using Eq. (29). The reader should note that the calculation of $\mathbf{P}^{-1}$ and its inversion are computationally very expensive, while the evaluation of Eq. (29) represents a trivial amount of computational effort.
- **iii.** An alternative solution, commonly named SOS/2, for Sum-Over-States/2, consists of expressing the second order energy as an explicit sum over states similar to the exact expression given by the RS perturbation theory. Within this approach, $\mathbf{P}^{-1}$ is constructed according to Eq. (28), but it is diagonalized instead of inverted. In the new basis, in which $\mathbf{P}^{-1}$ is diagonal, it is possible to express the second order energy as:

$$E^{(2)}=\sum\frac{\langle i'|H_1|a'\rangle\langle a'|H_1|i'\rangle}{E'_i-E'_a} \quad (30)$$

where $|i'\rangle$ are the eigenvectors of $\mathbf{P}^{-1}$ and E'_i its eigenvalues. This formulation is totally equivalent to Eq. (29) but can be used to explicitly analyse the contributions of different molecular orbitals to the shielding.

For simplicity, all the equations discussed above have been expressed in terms of the Molecular Orbitals (MO), but the reader should keep in mind that the actual calculation of the shielding constants normally requires one to rewrite the equations in the Atomic Orbitals (AO) basis or to transform the necessary two electron integrals from the AO basis into the

MO basis. This transformation is the most demanding part of the shielding calculations in terms of the CPU, storage and memory requirements. Direct methods for the solution of Eq. (21), which avoid the two electron integral bottleneck, provide great advances in our ability to compute shielding [106,107].

4.3. Finite perturbation theory

The perturbation schemes described in the previous section were based on approximations to the exact perturbation theory, the notion of Finite Perturbation Theory (FPT) or Finite Field Perturbation Theory (FFPT) is based on the direct use of Eq. (2) to calculate the shieldings. In the FPT approach the electronic energy of the system is calculated with and without the magnetic fields derived from the vector potential given by Eq. (4) and the derivatives of the energy with respect to the magnetic fields are estimated numerically by finite differences:

$$\sigma_{\alpha\beta}=\left(\frac{\partial^2 E}{\partial\mu_\alpha\partial B_\beta}\right)_{B_\beta=\mu_\alpha=0}\approx\frac{E(\Delta\mu_\alpha,\Delta B_\beta)-E(0,0)}{\Delta\mu_\alpha\Delta B_\beta}. \quad (31)$$

In Eq. (31) the values of ΔB_β and $\Delta\mu_\alpha$ are selected in such a way that they produce a large enough change in the electronic energy of the system to calculate the denominator in Eq. (31) with the desired precision without introducing higher order terms in the derivatives. Normally it is necessary to calibrate these increments for each MO method but this does not represent a significant problem for the application of Eq. (31) to calculate shieldings. The FPT method can be easily programmed; therefore, it can be used to calculate the shielding for any high order approximation to the electronic wave function without major modifications of the necessary computer programs. Its most serious disadvantage is the need of a complete Self Consistent Field (SCF) energy calculation for each component of each of the shielding tensors in the molecule. The FPT method is useful for highly correlated methods for which the algebraic expressions of the second order energy are not readily available.

4.4. Perturbation theory including correlation effects

When appropriate techniques to mitigate gauge origin problems (see Section 4.6) are used, the Hartree-Fock level calculations of shieldings have been successful, even when using relatively modest basis sets. For instance, the ^{13}C chemical shift tensors in sucrose, calculated using the GIAO method, agree with their experimental measurements with standard marginal deviations of 4.6 ppm and 2.7 ppm when using the STO-3G and 3-21G basis sets, respectively [108]. But also many cases have been documented in the literature in which the Hartree-Fock (HF) calculations produce fairly poor results even in the limit of very large basis sets. Examples of this behavior can be found for CO group, where the calculated HF value is −26.1 ppm and the experimental value 0.6 ± 0.9 ppm [109], in the systematic overestimation of the δ_{11} principal components of the ^{13}C chemical shifts tensors in olefinic and aromatic carbons [79] and in several other cases involving atoms with multiple bonds or lone pairs.

To correct these deficiencies, several attempts have been made to include dynamic electronic correlation in the calculations of shieldings. A complete discussion of the electronic correlation effects on shieldings is outside of the scope of this article. For further details the reader is referred to the comprehensive review by Gauss and Stanton [110]. In Table 3 we have entered a number of examples showing the importance of electronic correlation effects on the calculated shieldings. Note that these are probably the most accurate calculations of shieldings available today; in most cases the results have been obtained using extended basis sets near the Hartree-Fock limit. Unfortunately, the high

computational demands of the electron correlated methods make their application unfeasible for use in many important chemical and biochemical problems involving large molecules.

It is apparent from these results that the importance of the correlation effects is highly dependent on the bonding situation of the nucleus. For a single bonded nucleus the correlation effects are small to the point that it is not always possible to estimate their impact in improving the agreement with the experimental data without taking into account vibrational, medium and temperature corrections. The correlation effects are much more important for nuclei in multiple bonds, in which case the agreement between the experimental and calculated values shows a significant improvement upon adding electron correlation contributions. Unfortunately, due to the large computational resources needed most correlated methods are not applicable to the study of structural problems (see Section 4.5).

4.5. Density Functional Theory (DFT) of chemical shifts

The methods to calculate shieldings including the contributions of the electronic correlation described in the previous section do not provide a practical alternative for calculating shieldings in large molecules because they scale as N^5 to N^7, depending on the approximation, with the number of electrons, N, in the molecule. The development of effective Density Functional Theory (DFT) methods [111] that include electronic correlation effects has proved to be an important tool in the field of shielding calculations. Using the DFT theory, which scales as N^2, it is possible to calculate shieldings in molecular systems of practical interest including electronic correlation effects. Moreover, new DFT methods with linear scaling are becoming available and certainly these will provide further improvements in the performance of these methods to calculate magnetic shieldings [106,107,112] in large systems.

The derivation of the DFT theory of shieldings follows quite closely the derivations for the CHF approach and it is not necessary to repeat it here. A complete derivation of these theories has been presented by several authors [113–116]. The principal difference between different DFT methods is the selection of the exchange-correlation functional used in the calculations. Unfortunately there are no formal ways to calculate this functional using first principles but there is a vast literature on how to develop different types of exchange-correlation functionals [117–119]. In the following we restrict our discussion to the exchange-correlation functionals that have proven effective for the calculation of shieldings. In Table 4 we compare the RMS between experimental and calculated ^{13}C and ^{15}N NMR chemical shifts for several commonly used exchange-correlation functionals for the compounds studied by Cheeseman and co-workers [115,116].

It is apparent that except for the calculations done using the LDA (Local Density Approximation) functional [111], the DFT calculations are much better than the Hartree-Fock estimates and are closer to the values obtained for MP2 calculations. Two important observations derive from Table 4: first, the calculations are not very sensitive to the exchange-correlation functional used, except for the LDA approximation and second, DFT methods recover a significant portion of the electronic correlation effect and provide a viable alternative to calculate chemical shifts with accuracies close to those obtained with the much more expensive MP2 method.

Numerous DFT calculations of shieldings using different exchange correlation functionals have been reported. While many of these studies have attempted to develop the best functionals to calculate shieldings [120–123], careful evaluation of the literature indicates that most of the modern exchange-correlation functionals give shieldings of similar quality. It has become apparent that the shieldings are much less sensitive to the selection of the

exchange-correlation functional than other molecular properties. While from the pragmatic point of view the success of DFT calculations of NMR shieldings is unquestionable, as discussed in the recent review by Gauss and Stanton [110], significant question remain on the formal theoretical aspects of the DFT theory of shieldings.

4.6. Gauge independent algorithms to calculate shielding

As discussed above, the so called "gauge" problem in shielding calculations (or more precisely, the lack of gauge invariance of the calculated shieldings) is a consequence of using a finite basis in the expansion of the wave function or electron density. This necessary approximation leads to the inexact cancellation of the gauge dependent terms in the diamagnetic and paramagnetic contributions to the calculated shieldings. In the following we discuss the common ways used to develop better methods to mitigate the gauge problem in practical applications.

Under a gauge transformation given by

$$\mathbf{A}(\mathbf{r}) \rightarrow \mathbf{A}(\mathbf{r}')=\mathbf{A}(\mathbf{r})+\nabla\lambda(\mathbf{r}). \quad (32)$$

The exact electronic wave function in the presence of a vector potential, **A**, transforms as

$$\psi(\mathbf{A}')=e^{-i\Delta}\psi(\mathbf{A}), \quad (33)$$

where

$$\Delta=c^{-1}\sum_i \lambda(\mathbf{r}_i) \quad (34)$$

and $\lambda(\mathbf{r}_i)$ is a continuous function of the positions of the electron *i*.

For complete variational basis sets Eq. (33) is automatically satisfied, the energy of the system is gauge invariant and the electronic current derived from the wave functions is conserved, i.e $\nabla \cdot \mathbf{j} = 0$ [32,124]. For approximate wave functions it is possible to force the wave function to fulfill Eq. (33) by expanding the wave function in the so called London orbitals or GIAOs (Gauge Invariant or Including Atomic Orbitals):

$$\chi_p(\mathbf{r}, \mathbf{A})=\chi_p(\mathbf{r})e^{\frac{-i}{c}\mathbf{A}(\mathbf{R}_p)\cdot\mathbf{r}} \quad (35)$$

where $\chi_p(\mathbf{r})$ are real atomic orbitals (Slater or Gaussian functions) and $\mathbf{R}_p$ is the position of the center of the orbital $\chi_p(\mathbf{r})$. When the wave function is expanded in this type of function, the optimization performed when applying the variational principle occurs within the space expanded by orbitals of the kind given in Eq. (35), therefore constraining the search in such a way that only wave functions satisfying Eq. (33) are considered. As a consequence all the trial functions change from one gauge to another in the prescribed way such that the energy is invariant. Unfortunately, the use of GIAOs does not guarantee the conservation of the electronic current and that *a priori* there is no reason to expect better results when using this enforced gauge invariance of the energy. Fortunately, because the GIAOs are the first-order solutions to the one-electron, one-center uniform magnetic field problem, when $\chi_p(\mathbf{r})$ is the solution to the problem for $\mathbf{B} = 0$, they do, however, provide a more flexible basis to expand the wave function in the presence of a magnetic field. As a consequence, in practical applications calculations using GIAOs usually produce better results with smaller basis sets.

Several methods have been proposed to mitigate the gauge problem using this approach to make the results formally gauge invariant even for incomplete basis sets and to produce better results when using moderate sized basis sets. These methods have become the standard approach used to calculate shieldings in large and moderate size molecules. The most common methods, in addition to the GIAOs expansion discussed above, are: IGLO (Individual Gauge for Localized Orbitals) [27,75,76,125–127]; LORG (Localized Orbitals Local Origin) [128]; IGAIM (Individual Gauges for Atoms in Molecules) [129] and CSGT (Continuous Gauge Transformation) [130]. Finally, it is interesting to mention Geertsen's method [131], which gives a gauge origin independent formulation of the shieldings by using second-order perturbation theory to calculate its diamagnetic part. Unfortunately, while quite elegant, this formulation is not conducive to practical applications due to the difficulties associated with the calculation of second order properties.

The distributed gauge methods can be classified into several different types: those that use Individual Gauges for Localized Orbitals, IGLO and LORG (compared in Ref. [127]); those that use a formulation based on the current of the electron density and Bader's [132] topological atom in a molecule description (IGAIM); an empirical function for the Continuous Transformation of the Gauge Origin (CSGT); or finally, the GIAO method, which accomplishes the invariance of the results by using individual gauge origins for each atomic function in the basis set. Methods using a localized orbital description, such as LORG and IGLO, can provide a somewhat intuitive decomposition of the shielding into contributions arising from different localized orbitals, a feature quite appealing to chemists. The IGAIM method provides a decomposition of the shieldings into contributions arising from the electronic density of each atomic basin, as defined by Bader's topological atom in a molecule description [132]. These types of decompositions are not available when using the GIAO or the CSGT methods, but the latter provides a three-dimensional representation of the distribution of induced electron current. While the methods discussed above take different approaches to mitigate the gauge problem, all of them are exact and converge to the same shielding values in the limit of very large basis [113]. Of course, the converged values are identical to those obtained with the common origin method when the same extended basis is used in the calculations. In Fig. 4 we present the basis set dependence of calculated chemical shifts in glycine for different distributed gauge methods compared with the results obtained using the common origin method. The calculations were done using the Gaussian 98 system, the basis sets used correspond to the Dunning's correlation consistent basis, which includes polarization functions [133] and the standard STO-3G from Pople et al. [134].

It is apparent from Fig. 4 that when using the smallest basis set, STO-3G, none of the methods is able to recover a significant fraction of the results for the infinite basis limit. Significant improvements are observed when using the double zeta (DZ) basis set. Finally, the calculated values for all the methods considered here are almost identical when the quadruple zeta (QZ) basis set is used. While it appears in Fig. 4 that the IGIAM method converges faster than the GIAO method, to the author's knowledge this is not a general conclusion. For instance the opposite results have been reported by Cheeseman et al. [115] in other compounds.

5. Intermolecular effects on shielding

In this section we review the intermolecular interactions that affect the magnetic shielding and how they change the measured chemical shifts and consequently affect the comparison of experimental and calculated values. We present some basic principles and discuss how these effects can be taken into account and calculated. The intermolecular effects on shielding have their origin in the same physical principles in any phase, but the analysis of

the data and the computational models to describe the effects are quite different. Gas phase effects have been extensible studied by Jameson and co-workers [136–139]. They have been very useful in providing an understanding of the isotope effects observed in chemical shifts, but they provide very limited information about structural issues and will not be discussed in this review. In the following we concentrate on issues related to the intermolecular effects in condensed phase, solution and solid state.

5.1. Intermolecular effects in solution

The solvent effects on the shielding were recognized many years ago. As early as 1960 Buckingham and co-workers [140,141], classified the different mechanisms that contribute to the solvent effect observed in solution NMR experiments. The different effects according to the Buckingham classification are

$$\sigma=\sigma_0+\sigma_s=\sigma_0+\sigma_b+\sigma_a+\sigma_W+\sigma_E, \quad (36)$$

where σ_0 is the ro-vibrationally averaged shielding for the isolated molecule and σ_s is the solvent contribution that is composed of four contributions, σ_b corresponds to the bulk magnetic susceptibility of the sample that affects all nuclei in the same way and that can be easily discounted by using internal referencing; σ_a is the contribution from the anisotropy in the magnetic susceptibility of the solvent molecules dominated by the short range steric repulsive forces; σ_W is the contribution due to the van der Waals interactions and σ_E is the long range contribution from the electric field generated by the solvent molecules. This theoretical framework is still in use today to analyse the solvent effects on the magnetic shielding. The actual calculation of these effects is quite challenging because any model that attempts to represent these interactions has to take into account both the electromagnetic iterations generated by the solvent molecules as well as their dynamics. The topic of intermolecular interactions affecting the magnetic shielding in solution has been the subject of several reviews, see for instance [91,142,143] and the most recent and comprehensive one is by Bagno et al. [144]. The theoretical methods in use to model the intermolecular effects on the magnetic shielding in solution can be generally classified into continuous models that represent the solvent as a continuous uniform media, including its properties as producing an average field and discrete methods based on an atomistic description of the solvent where the motional characteristics of the solvent are given by Molecular Dynamics (MD) simulations. One of the most common continuous models is the solvaton model introduced by Germer [145] where the system is modeled as a solute molecule surrounded by the charges (solvatons) induced in the target molecule. The model has been coupled to several Quantum Mechanics (QM) methods in order to calculate magnetic shielding, these include the empirical INDO/S [92], and several *ab initio* packages like Gaussian 09, ADF and Dalton (see references and descriptions of these programs in Section 6). Discrete methods typically couple classical MD simulations, from which representative ensembles of the solvent molecules surrounding the solute are chosen and included into the QM calculations of the shielding. The final shieldings are calculated as the average of those calculated for each of these ensembles [146,147]. While the cost of calculations using continuous models is almost the same as for the isolated molecule, the cost of calculations using discrete methods greatly increases with the number of solvent molecules explicitly included in the QM calculations. A detail discussion to these issues can be found in Ref. [144].

5.2. Solid state effects

In most cases there are no or only very minor differences between the isotropic chemical shifts measured in solution (in a non-polar solvent) vs. those measured in the solid state either in a MAS (Magic Angle Spinning) spectrum or from the average of a measurement of

the principal values of the chemical shift tensor [22]. When this is the case, it is an indication that intermolecular effects are probably not an important factor in the system under study and that there are no crystal effects complicating the interpretation of the SSNMR (Solid State NMR) spectra. Often in these cases there is also good agreement (typically within 5 ppm for the principal values) between the experimental chemical shift values and the results of calculations done on a single isolated molecule. However, there are many examples in the literature where substantial differences are measured between solution and solid state chemical shifts and/or between experimental solid state data and single molecule theoretical measurements. In some cases these differences in the isotropic chemical shift values are of such magnitude that duplication of lines may be observed in the SSNMR spectra. When such differences are observed one must look to the structure of the molecule and its local environment for reasons to explain the differences. Some of the differences are due to changes in the molecule itself (structure and/or dynamics) upon going from solution/liquid to solid, while others are due to strong intermolecular interactions in the solid state. The main contributions to solid state effects are described in a recent review [148] and include:

conformational and tautomeric averaging;

crystal symmetry;

multiple molecules per asymmetric unit;

presence of polymorphs;

multiple solid state phases;

electrostatic effects;

hydrogen bonding;

magnetic effects.

5.2.1. Theoretical methods used to calculate solid state effects—As stated in the previous section, there are numerous mechanisms that can explain the changes observed between the NMR chemical shifts measured in solution vs. those determined in a solid phase. While the experimental measurements can provide unequivocal evidence of the existence of solid state effects on chemical shifts, the experiments alone seldom can provide conclusive information on their chemical and/or structural origins. Theoretical and computational methods play a fundamental role in interpreting the experimental results and provide insight into the physical origin of the solid state effects. This is possible because the calculations are able to test a variety of models, each of which can selectively include different plausible mechanisms that may be responsible for the solid state effect observed in the chemical shifts.

The theoretical methods available to take into account intermolecular interactions can be classified in mainly two categories: those that represent the intermolecular interactions by an electric or magnetic field that mimic the interactions generated by the rest of the molecules in the crystal; and those that explicitly treat the neighboring molecules. Most of the methods in the first category use either a finite distribution of charges or a series of multipoles to represent the electric field generated by the environment [73,149–156]. Recently it has been shown that it is possible to observe purely magnetic intermolecular effects [157] and in this case the use of NICS [158–160] (Nucleus Independent Chemical Shielding) calculations have been used to take into account these effects [161]. The second category of methods available treats the neighboring molecules explicitly in the quantum mechanical calculations of the chemical shielding. For a number of years the explicit representation was accomplished by including a finite number of neighboring molecules in the calculations.

This approach is usually described as “cluster model.” The greatest disadvantage of the “cluster model” methods is that their computational costs increases rapidly with the number of neighboring molecules included in the calculations. To avoid this problem a number of combinations of cluster and electrostatic models have been used over the years; in these hybrid models the closest neighbors are explicitly represented and the more remote ones are replaced by an approximate field.

5.2.2. Shielding calculations using periodic boundary conditions—In recent years several research groups have reported new theories that allow the calculation of shielding in systems with Periodic Boundary Conditions (PBC). These theories eliminate the need of using the inherent approximations of the cluster and electrostatic methods by including in the calculations all the interactions arising from the crystal field. Sebastiani and co-workers [162–167] implemented their method in the popular CPMD program [168]. Sebastiani proposed the use of localized Wannier orbitals and a periodic pseudo position operator with a saw-tooth shape. This method can be used to calculate shielding in both isolated and full periodic systems. A similar theory was presented by Mauri et al. [169] in which the problems associated with the lack of definition of the position operator in periodic systems has been resolved by using a modulated external magnetic field; they calculate the shielding by numerical differentiation of the values calculated for two small, but not zero, wave vectors. This method, as well as the one from Sebastiani, has been implemented using pseudo potentials and therefore cannot take into consideration the contribution of the inner shells. This approximation can be problematic for non-first-row nuclei and in a subsequent paper Pickard and Mauri [170] introduced the GIPAW (Gauge Including Projector Augmented Wave) method that formally includes the contribution of the core electrons when using pseudo potentials. Numerous applications using this method have been presented [43,169–180]. Recently the same methods have been implemented in the Quantum Espresso code [181].

6. Software and hardware for quantum mechanical calculations of shielding

Significant shielding calculations can be done using hardware and software commonly available in most structural chemistry labs. With this in mind, it is important to provide a short account of the software available and the hardware necessary for NMR shielding calculations. Here we describe several of the most common software packages that can be used to calculate shieldings and the typical hardware required for these calculations. The reader should notice that the software list is not comprehensive and that at the time of writing this review the calculation of NMR properties is becoming a standard feature of most QM packages.

Gaussian 09 (http://www.gaussian.com/)

In terms of making shielding calculations available to a large community of researchers, the most significant development in recent years has been the work by Cheeseman et al. [115]. Using the framework of the CDFT (Coupled DFT) perturbation theory, they implemented the calculation of shielding tensors in the popular Gaussian suite of programs [182]. This implementation makes use of the techniques previously developed by Pulay and coworkers [183,184] and co-workers to efficiently calculate the complex two electron integrals necessary to implement the GIAO formulation. This method has become the most popular tool for calculating shieldings.

A number of additional methods used to calculate shieldings have also been implemented in the Gaussian suite of programs in recent years. These include HF, DFT and MP2 electronic approximations as well as single origin, GIAO, IGAIM and CSGT methods to deal with the gauge origin dependence problem.

ACESII **(http://www.qtp.ufl.edu/Aces2/)**

Provides capabilities to evaluate analytically NMR shielding tensors at the SCF and MBPT(2) levels using Gauge Including Atomic Orbitals (GIAOs) to ensure exact gauge-invariance.

DALTON **(http://www.kjemi.uio.no/software/dalton/dalton.html)**

This software can calculate NMR properties (both magnetizabilities, nuclear shieldings and all contributions to nuclear spin–spin coupling constants) and EPR properties (electronic g-tensor, hyperfine coupling tensor and zero-field splitting tensor) at the HF/DFT/MCSCF levels of approximation.

CADPAC **(http://ket.ch.cam.ac.uk/software/cadpac.html)**

NMR shieldings can be calculated using the LORG algorithm for the DFT and HF electronic approximations.

Jaguar **(http://www.schrodinger.com/products/14/7/)**

Allows the calculation of NMR properties using HF, DFT and other highly correlated methods.

deMon **(http://www.sims.nrc.ca/sims/deMon/)**

This software has implemented the calculation of NMR shieldings using the DFT approximation within the SOS scheme described by Malkin et al. [185].

NWChem **(http://www.emsl.pnl.gov:2080/docs/nwchem/nwchem.html)**

This software has implemented the calculation of NMR shielding (GIAO method) for the HF electronic approximation using the coupled Hartree-Fock scheme and DFT methods.

PQS **(http://www.pqs-chem.com/ible)**

This software was known in the past as the Texas program by Peter Pulay [183]. Nuclear magnetic shieldings for closed-shell HF and DFT wave-functions can be calculated for common gauge and GIAO gauge choices. The program has been parallelized to run in computational clusters.

ADF **(http://www.scm.com/)**

The Amsterdam Density Functional Package is being developed at the well-known theoretical chemistry groups of Baerends, Ziegler, Snijders, and by several other scientists worldwide. This package can calculate NMR chemical shifts and spin–spin couplings using density functional theory, including relativistic corrections using the ZORA approximation [48].

CPMD **(http://www.cpmd.org/)**

The Carr–Parrinelo molecular dynamics code has implemented the theory required to calculate NMR shielding for periodic system reported by Sebastiani and Parrinello [166].

CASTEP (DFT/GIPAW) **(http://www.castep.org/)**

This software has implemented the GIPAW method presented by Mauri and co-workers [78,169,170].

Quantum Espresso (http://www.quantum-espresso.org/)

This package has implemented DFT/GIPAW calculations using the GIPAW method [78,169,170]. This code is available as an open source license [181].

Modest shielding calculations, in systems with up to 10–20 non-hydrogen atoms and using a few hundreds of basis functions can be carried out in a reasonable time using typical desktop computers. While these calculations cannot be done in an interactive fashion, overnight runs for each shielding calculation are a reasonable expectation. If a geometry optimization of the molecule is necessary before performing the shielding calculation, this time may increase significantly depending on the quality and magnitude of the geometry optimization needed. Much larger calculations are more suitable for large clusters or other parallel supercomputer systems. For instance using 8 processor cores (2.8 GHz) a calculation of the shieldings for a molecule with 40 atoms takes approximately 1 h, while a calculation for a molecule with 100 atoms may take a day.

7. Expected accuracy of quantum mechanics based chemical shift calculations

The methods used to calculate chemical shifts have achieved a degree of maturity that may allow non-computational chemists to use these methods to aid in their experimental efforts. In the following we present a number of comparisons between calculated and measured chemical shifts that can be used by practitioner chemists to assess the expected accuracy of the calculations and make appropriate decisions on the merits of using them to clarify or enhance their interpretation of experimental results. For the purpose of this section we will concentrate on chemical shift calculation using the DFT approach because this method has become the work-horse of chemical shift calculation for organic molecules containing first and second row atoms. In the following we provide a general overview of the quality of results that can be obtained routinely when using the popular B3LYP [186], MPW1PW91 [187] and OLYP [188] exchange-correlation functionals for shielding calculations in medium size organic molecules from the G2 and G3 standard sets [189,190]. The calculations were made [191] with the popular Gaussian 03 system for molecular modeling [192], using the GIAO [184], CSGT [130] and IGAIM [129] approaches to enforce the gauge invariance and Dunning's d95** basis sets [133]. In all cases the calculations were performed using the optimized (mp2(full)/6-31g*) geometries that are available for the molecules in the G2 and G3 data sets (http://www.cse.anl.gov/Catalysis_and_Energy_Conversion/Computational_Thermochemistry.shtml). From the molecules selected for the shielding calculations we have included in the analysis presented here 244 ^{1}H shieldings, 133 ^{13}C shieldings, 18 ^{15}N shieldings and 26 ^{17}O shieldings.

Figs. 5–8 and Tables 5–8 depict the correlation and the correlation parameters between the calculated shieldings and their corresponding chemical shifts. In the tables the slope, intercept and standard deviation of the linear fits are given. Deviations of the values of the slopes from the ideal value of minus one (except for ^{15}N where it is one), provide an estimate of the systematic errors in the calculations that are usually attributed to the deficiencies in the way that the electron correlation is taken into account. In general the values of the intercept are less informative because it is widely accepted that there are large uncertainties in determining absolute shieldings of reference compounds.

As depicted in the previous tables and figures the methods considered here are able to predict the ^{1}H chemical shifts with relative accuracies of 2–3%, with slopes that are independent of the exchange-correlation functional used varying from 10% (GIAO) to 20% (IGAIM and CSGT). For ^{13}C the results are also quite satisfactory, providing relative accuracies of 1.4–1.9% and slopes different from minus one by less than 6%. A clearer

indication of deficiencies of these methods becomes apparent for ^{15}N and ^{17}O shieldings, where the standard deviations reach ~10% and ~14%, respectively. Also significantly larger deviations in the slopes are observed for these nuclei, up to 20% ^{15}N and up to 8% for ^{17}O. However, in these cases the agreement can also be reduced by well-known medium effects on these experimental chemical shifts [193] that are not taken into account in these calculations. The results presented here to illustrate the agreement between calculated and experimental isotropic chemical shifts represent a best case scenario because it has been recently documented that fortuitous cancellation of errors in the individual tensor components of the calculated shieldings can lead to artificially high agreement in the isotropic chemical shifts [16].

The comparison of calculated and experimental principal values or even better the full shielding tensors can provide a more rigorous assessment of the quality of the calculations. One of the most rigorous analyses of the accuracy of NMR calculations has been performed by Iuliucci et al. [16,17] where a set of 102 ^{13}C chemical shift tensors, measured in single crystals from a series of aromatic and saccharide molecules for which neutron diffraction data are available, is used to survey models based on Density Functional (DFT) and Hartree-Fock theories. The quality of the models is assessed by their least-squares linear regression parameters. It is observed that, in general, density functional theory outperforms restricted Hartree-Fock (HF). For instance, Becke's three parameter exchange correlation B3LYP [186] method as well as the MPW1PW91 [187] method generally provide the best predicted shieldings for this group of tensors. However this performance is not universal, as none of the DFT exchange correlation functionals can predict the saccharide tensors better than HF. Both the orientations of PAS as well as the magnitude of the shielding were compared using the chemical shift distance in the icosahedral representation defined by Alderman and co-workers [194] to evaluate the quality of the calculated individual tensor components. In the icosahedral representation the three principal components of the shielding tensor together with the three direction cosines are transformed into six icosahedral shielding tensor elements, which can be used to compare shielding tensor orientations and principal values on the same footing avoiding the artifacts introduced when the tensors are represented as principal values and directional cosines. Systematic shortcomings in the prediction of the principal components were observed, but the theory predicts the corresponding isotropic value more accurately. This is because these systematic errors cancel, thereby indicating that the theoretical assessment of shielding predictions based on the isotropic shift should be avoided. The results are depicted in Fig. 9.

8. Applications of chemical shifts calculations

The use of NMR calculations to complement experimental measurements to solve structural problems is wide-spread in the literature; it is not practical to try to present here a comprehensive list of all the applications that have been reported, even recently, in the literature. In the following sections we present a very limited number of examples on how shielding calculations, which now can be performed almost routinely, can complement experimental measurements to solve structural problems. We have classified the examples in general categories that may help the reader to easily find examples relevant to his or her research problem, but we acknowledge that this classification is somewhat arbitrary because in many cases the calculations are used in the same paper for multiple purposes.

8.1. Molecular conformation of organic molecules

Wang et al. [195] have measured and calculated, using the GIAO at the B3LYP/6-311++G** approach, the NMR chemical shifts for three monoterpene diastereomers produced by the walkingstick (Anisomorpha buprestoides). By taking into account the Boltzmann distribution of conformers, the authors were able to distinguish between conformers present

and absent in the sample. To improve its ability to distinguish the stereoisomers, they utilized both ^{1}H and ^{13}C chemical shift information by defining combined root mean-square deviation (cRMSD) as:

$$cRMSD=RMSD(^{13}C)+10\times RMSD(^{1}H). \quad (37)$$

The use of this combined information significantly enhances the predictive power of the calculated chemical shifts. The conformational information obtained from the comparison between calculated and experimental chemical shifts is consistent with that obtained from the analysis of the calculated relative energies and distances measured by interproton NOEs and distance calculations [195].

Belostotskii [196] presented a conformation study of haouamine A (I), Fig. 10, based on the comparison of the calculated (B3LYP/6-31+G(d)//GIAO) and measured chemical shifts. This is one of the larger applications of this methodology because haouamine A (I) is much more stereodynamically complex than the small models used to validate previous chemical shift based conformational studies. A total of 16 rotamers were considered in this study, for which the chemical shifts were calculated for their optimized geometries. The comparison of the ^{13}C chemical shifts was able to identify two conformers that fit the experimental data. This is considerably better than the results that can be obtained by the simple analysis of the energetics of this compound. The authors conclude that this method can be successful for any case in which the ^{13}C chemical shifts stereoisomers are separated by more than 2 ppm.

Härtner and Reinscheid [197] presented correlations between experimental and calculated ^{13}C chemical shifts in a series of menthol diastereomers. In this way the authors showed that identification problems with newly isolated natural products can be solved. Starting from simulated, low energy conformers of menthol, neomenthol, isomenthol, and neoisomenthol the ^{13}C chemical shifts were obtained using DFT calculations, B3LYP/6-31G(d,p), and the large differences in chemical shifts observed for the prochiral Me groups of the isopropyl substituent of menthol could be differentiated using the correlations between experimental and calculated values. The sensitivity of the chemical shifts to the molecular conformation can be observed in Fig. 11, and the agreement between experimental and calculated values can be used to determine experimental conformations. The results presented in this paper were also supported by energy calculations and the measurement of the $^{1}J_{CH}$ and $^{3}J_{HH}$ coupling constants.

These three examples show how chemical shielding calculations in organic molecules ranging from fairly small hydrocarbons to alkaloid like haouamine are useful for studying their conformational properties. Because the calculations predict the chemical shifts with sufficient accuracy, it is possible to extract important conformational information from the comparison between the experimental chemical shifts and the calculated values, which are greatly influenced by the molecular conformation and geometry used in the QM calculations. Ideally this could be formulated as an inverse fitting problem, but the computational time required for quantum mechanical chemical shift calculations is still a barrier for such an approach. Recent studies using solid state NMR to study the conformation of organic and pharmaceutical molecules have been reviewed by Potrzebowski [198].

8.2. Biological molecules

The use of chemical shift information to solve structural problems in biological molecules was demonstrated many years ago [97]. The main limitation has always been the computational capabilities required to perform chemical shift calculations in very large

biological molecules. In recent years the advances in computer power have allowed researchers to perform more rigorous studies, but in general these studies are performed on model systems that represent fragments of interest in biological molecules. For instance Zienau et al. [199] studied the molecular recognition mechanism in molecular tweezer systems using the model depicted in Fig. 12. Since ring-current effects are particularly important in this system, quantum mechanical calculations in the model system were used to show that intermolecular interactions strongly influence the corresponding proton chemical shifts by up to 6 ppm. The quantum chemical results allowed them to reliably assign the spectra and to gain information both on the structure and on the importance of intra- and intermolecular interactions present in these molecular tweezers.

Souma et al. [200] optimized a right-handed α-helix (αR-helix) structure of sequential 18-mer copolypeptide H-(Ala-Gly)9-OH (C45H74N18O19) using the B3LYP/6-31G(d) approach and then calculated the chemical shieldings of the optimized structure using the B3LYP/6-311G(d,p) method. As a result, they confirmed highly accurate conformational parameters characteristic to the αR-helical H-(Ala-Gly)9-OH, which were identical with those of the individual Ala and Gly residues. Most of these parameters were fundamentally the same as those obtained for the optimized αR-helical H-(Ala)1.

In a series of landmark studies, Vila et al. [201–203] demonstrated how calculated $^{13}C_{\alpha}$ chemical shifts can be used to elucidate protein structure, opening a new and very important avenue for tackling this very important problem. The method is based on the realization that it is possible to calculate the $^{13}C_{\alpha}$ chemical shifts in a protein by calculating them in the fragment Ac-G-**X**-G-NMe, where **X** is the residue under consideration [203]. The method [202] uses simultaneously the chemical shift information and the usual NOE data in an iterative fashion to find the best structure that can match both the NOE and chemical shifts constrains. The method has been tested by performing a blind test [201] on a set of 20 NMR-derived conformations of a 48-residue all-α-helical protein (PDB ID code 2JVD), and the validation was performed by comparing the observed $^{13}C_{\alpha}$ chemical shifts with those computed at the density functional level of theory.

In contrast with the use of chemical shift calculations to elucidate the conformation of organic molecules, the work on biological molecules involves the selection of critical fragments representing the parts of the molecule of biological interest [204,205]. These fragments have to be selected using the criteria of plausible representation of the biologically interesting fragments but also limiting their size such that it is possible to perform quantum mechanical calculations. In contrast with MD simulations [206] that commonly use empirical potentials and can address very large molecular systems, chemical shift calculations require quantum mechanical calculations which are much more computationally expensive and, therefore, they limit the size of systems that can be studied. The emergence of linear scaling methods [106] may allow calculations in biologically relevant systems without using the fragment approach in the near future [207]. Alternatively, as discussed above, it is still possible to use an empirical approach based on extensive data collection [101]. Recent solid state NMR applications to structural biology have been reviewed by Middleton [208].

8.3. Disordered systems

Structural elucidation in disordered materials has been a significant challenge for many years, while powder diffraction techniques have made substantial advances in recent years [209]. Solid state NMR still plays a critical role in this field. Applications of chemical shifts calculations in disordered polymers were reported many years ago and continue to provide improved methods [210–214] for their structural analysis. In recent years new developments in solid-state NMR techniques have allowed researchers to acquire high resolution NMR

spectra for solid systems with structural disorder at much higher resolution; however, the structural origin of the observed chemical shift nonequivalence in these systems cannot be inferred from the experimental data alone. Ling and Zhang [215] reported a quantum chemical investigation of the solid-state NMR spectrum in N,N-bis(diphenylphosphino)-N-((S)-α-methylbenzyl)amine, where eight different ^{31}P NMR chemical shifts can be observed in the spectra within a range of 13.0 ppm. Results from quantum chemistry methods using optimized geometries and including solid state effects lead to the excellent correlation observed in Fig. 13. This high level of agreement (SD = 1.1 ppm, $R^2 = 0.949$) allows at least a tentative assignment of the phosphorous atoms in the unit cell based on the quantum chemical calculations.

8.4. Nano structures

NMR shielding calculations were reported early on for C_{60} and other fullerenes [216]; calculations in these type of compounds have been reviewed by Orendt [217]. In recent years as computational resources and methods improved, much larger calculations on structures of interest to nano materials have been reported. A comprehensive list of these studies is beyond the scope of this review, however one example is a first-principles calculation of ^{13}C NMR chemical shifts in infinite single-walled carbon nanotubes performed by Lai et al. [218]. Using the density functional theory with periodic boundary conditions the authors calculated the ^{13}C NMR isotropic chemical shifts of the semiconducting and semimetallic infinite Single-Walled Carbon Nanotubes (SWNTs). The ^{13}C chemical shifts of SWNTs with the diameter smaller than 1.4 Å can be classified into two distinct groups according to their electronic structures: the semiconducting group and the semimetallic group. The chemical shifts of the semiconducting group decrease monotonously with the increasing nanotube diameter and are 0–12 ppm larger than those of their semimetallic counterparts in the typical diameter range (1.05 ± 0.2 nm) of SWNTs produced by the common high-pressure CO decomposition method (HiPCO). The chemical shifts of the two groups overlap around the diameter of 1.4 Å and the chemical shift of the semimetallic group becomes larger than that of the similar-sized semiconducting group as the diameter is larger than 1.4 Å. The chemical shifts of the four examined helical SWNTs are very close to those of the zigzag SWNTs with similar diameters and electronic structures. These findings are presented in Fig. 14.

8.5. Studies in coals

The calculation of ^{13}C NMR shielding tensors has played an important role in the determination of coal structure and aromaticity [219–221]. For instance this approach has been used to study two anthracite coals and a fuslnite maceral by powder pattern line shapes analysis. The best fits, depicted in Fig. 15, are a superposition of three different bands due to benzene like, condensed (bridgehead and inner) and substituted carbons. Theoretical calculations on circumcoronene used as a model compound support these interpretations of the experimental data. The calculated tensor values are critical in arguing that the multi component fit in Fig. 15 is physically plausible and not a simple artifact of the curve-fitting process. The ratio of nonprotonated to protonated aromatic carbons obtained on anthracites by the spectroscopic analysis is also in excellent agreement with the elemental analysis and previous studies by dipolar dephasing NMR techniques. The method therefore is a valuable way of analysing the structure of high-rank coals and should be useful in char characterization.

8.6. Studies of stereochemistry

The reliable determination of stereocenters contained within chemical structures usually requires utilization of NMR data, chemical derivatization, molecular modeling, quantum-mechanical (QM) calculations and, if available, X-ray analysis. These are laborious and

expensive techniques; recently Elyashberg et al. [223] demonstrated that the number of stereoisomers that need to be thoroughly investigated can be significantly reduced by the application of NMR chemical shift calculations to the full set of possible stereoisomers. The authors show that from all the $2^5 = 32$ stereoisomers generated for artarborol by using a fragmental approach based on HOSE codes [224], the constrains imposed by the calculated ^{1}H and ^{13}C chemical shifts leave only four (Fig. 16) possible candidates to be analysed further, with a considerable reduction of the effort needed for the determination of the observed stereoisomers.

8.7. NMR crystallography

The examples discussed above give a clear indication of the great potential for using NMR chemical shifts for structure elucidation. The strong sensitivity of the chemical shifts to molecular structure [79] is the basic property that make this possible. The examples also show that the relationship between structure and chemical shift is not simple. In contrast with the simple relationship between structure and NOEs given by the $1/r^6$ dependence on the distance between nuclei or even the reciprocal lattice relationship between X-ray or neutron diffraction patterns and molecular structure, the relationship between chemical shift and molecular or crystal structure is mediated by the complex quantum mechanical machinery presented in previous sections of this review. Consequently, until recently most applications used *ad hoc* approaches like those described above. In recent years, we have seen a consistent effort by several research groups to develop systematic ways to obtain molecular and crystal structures using NMR chemical shifts. This emerging field has been named “NMR Crystallography” [80]. While it is recognized that solid state NMR cannot be competitive with diffraction methods when single crystals are available, the methodology has been shown to be competitive with powder diffraction and other techniques commonly used when single crystals are not available. Although even when single crystals are available, SSNMR techniques can be very competitive with X-Ray Diffraction (XRD) in locating H atoms [10]. In this section we provide a brief account of some of the advances in this field; a comprehensive report on the state of the art of the field was provided recently [80,225].

Using the principles of NMR crystallography, Meejoo et al. [226] studied the structure of the β-polymorph of (*E*)-4-formylcinnamic acid. The structure refined as an ordered structure using the powder diffraction spectra led to a high quality structure, but the high resolution solid-state ^{13}C NMR spectrum of this material showed evidence of disorder of the formyl group. When using the information of the disorder of the formyl group into the refinement, the Rietveld quality factors, R_{wp}, improved from $R_{wp} = 3.27\%$ to $R_{wp} = 2.87\%$. The results of this important contribution to the field NMR crystallography are summarized in Fig. 17.

Witter et al. [227] studied the ^{13}C chemical shift resonances of bacterial cellulose by solid state NMR and performed a constrained crystal structure refinement. The solid-state NMR assignments of the ^{13}C resonances of bacterial cellulose Iα were reinvestigated by INADEQUATE (Incredible Natural Abundance Double Quantum Transfer Experiment) experiments on uniformly ^{13}C-enriched samples from *Acetobacter xylinum*. The authors determined the principal components of the chemical shift tensors of each ^{13}C labeled site from a 2D iso-aniso RAI (Recoupling of Anisotropy Information) spectrum acquired at a Magic Angle Spinning speed of 10 kHz. On the basis of these NMR data, the crystal structure of cellulose Iα was refined using the ^{13}C chemical shifts as target functions. Starting off with the coordinates derived from neutron scattering [228] and using molecular dynamics simulations, a total of 800 structures were selected for further consideration. These structures were subsequently optimized within the given isotropic chemical shift constraints and applying crystallographic boundary conditions in the shielding calculations. The resulting four model structures that best fit the NMR data were then assessed by

simulating the chemical shift tensors, using the bond polarization theory, and comparing these values with the experimental chemical shift anisotropy information obtained by RAI spectra. The earlier neutron diffraction study had reported two possible occupation schemes for the hydrogen-bonded hydroxyl groups that connect the cellulose chains. From these two possibilities, the NMR results single out one pattern as the most probable structure, which is compared with the neutron structure in Fig. 18. The extraordinary improvement observed in the calculated chemical shifts when using the NMR optimized structure when compared with that obtained using the neutron diffraction data is depicted in Fig. 19.

Grant and co-workers have presented a combined solid-state NMR and synchrotron X-ray diffraction powder study on the structure of the antioxidant (+)-catechin 4,5-hydrate [229]. As in the case of cellulose there is a marked improvement in the agreement between calculated and experimental chemical shifts upon refining the crystal structure using the NMR information. This is depicted in Fig. 20.

Following the previous studies of solid-state polymorphism in 10-deacetyl baccatin III [230] the Grant group presented the structural characterization of a new anhydrous polymorph of paclitaxel (see Fig. 21) based on solid-state NMR and X-ray powder diffraction methods [231]. The three-dimensional structure of this unique polymorph of the anticancer drug paclitaxel (Taxol®) was established using solid state NMR tensor (^{13}C and ^{15}N) and heteronuclear correlation (^{1}H–^{13}C) data. The polymorph has two molecules per asymmetric unit ($Z' = 2$) and is thus the first conformational characterization with $Z' > 1$ determined solely by SSNMR. Experimental data was correlated with structure through a series of computational models that extensively sampled all possible conformations of the molecules. For each computational model, corresponding tensor values were computed to supply comparisons with experimental information, which, in turn, establishes the paclitaxel's new polymorph structure. Heteronuclear correlation data at thirteen key positions provided shift assignments into the asymmetric unit for each comparison. The two distinct molecules of the asymmetric unit possess nearly identical baccatin III moieties with matching conformations of the C10 acetyl moiety and, specifically, the torsion angle formed by C30–O–C10–C9. Additionally, both are found to exhibit an extended conformation of the phenylisoserine side chain at C13 with notable differences in the dihedral angles centered around the rotation axes of O–C13, C20–C10 and C30–C20. The best structures encountered by SSNMR are presented in Fig. 22.

9. Conclusions

Chemical shift calculations are possible in very large systems of real chemical interest and they can provide accuracies that are sufficient to explore molecular and crystalline structural features in great detail. In some cases the errors in the calculations are even comparable to the errors observed in experimental values. The calculations can be done both on isolated molecules and on crystals using periodic boundary conditions. The great advances in the calculation of NMR shieldings coupled with the extreme sensitivity of the shielding on the molecular and crystalline structure led to the recent establishment of the field of NMR crystallography, which shows great promise as a premier structural analysis tool for material that exhibit disorder as well as for those where large high quality single crystals are not available. Unfortunately, most of the work in NMR crystallography is performed using *ad hoc* methods and lacks a definite integration of different refinement methods. Development of software that incorporates both diffraction and NMR refinement in a consistent framework can be of great importance in propelling the use of NMR crystallography to a larger user community.

Acknowledgments

Support from the National Science Foundation, The National Institutes of Health and the Office of Science of the Department of Energy, which over the years have provided funding for the NMR program at the University of Utah, is gratefully acknowledged. Discussions with our colleagues in the NMR lab, especially Prof. David M. Grant, greatly contributed to furthering our understanding of chemical shifts. The author acknowledges the many years of collaboration with Prof. David M. Grant and his associates, especially Profs. Anita Orendt, Ron Pugmire, Don W. Alderman Robbie Iuliucci and Mark S. Solum with whom he developed most of the material and ideas presented in this article. The Center for High Performance Computing at the University of Utah continues to provide computer resources.

Glossary of abbreviations

AO	Atomic Orbital
CHF	Coupled Hartree-Fock
CSGT	Continuous Gauge Transformation
DFT	Density Functional Theory
FFPT	Finite Field Perturbation Theory
FPT	Finite Perturbation Theory
GIAO	Gauge Including Atomic Orbitals
GIPAW	Gauge Including Projector Augmented Wave
HF	Hartree-Fock
IGAIM	Individual Gauges for Atoms in Molecules
IGLO	Individual Gauge for Localized Orbitals
INADEQUATE	Incredible Natural Abundance Double Quantum Transfer Experiment
IUPAC	International Union of Pure and Applied Chemistry
LDA	Local Density Approximation
MAS	Magic Angle Spinning
MCSF	Multi Configuration Self Consistent Field
MD	Molecular Dynamics
MO	Molecular Orbital
MP(2)	(3), …, Møller–Plesset Perturbation Theory of Order (2), (3), …
NICS	Nuclei Independent Chemical Shifts
NMR	Nuclear Magnetic Resonance
PBC	Periodic Boundary Conditions
QM	Quantum Mechanics
RAI	Recoupling of Anisotropy Information
SCF	Self Consistent Field
SSNMR	Solid State Nuclear Magnetic Resonance
SWNT	Single Wall Nano Tubes
TALOS	Torsion Angle Likeliness Obtained from Shift and Sequence Similarity
XRD	X-Ray Diffraction

ZORA Zero Order Regular Approximation

References

1. Purcell EM. A precise determination of the proton magnetic moment in Bohr magnetons. Phys Rev. 76(1949):1262–1263.
2. Purcell EM, Torrey HC, Pound RV. Resonance absorption by nuclear magnetic moments in a solid. Phys Rev. 1946; 69:37–38.
3. Ramsey NF. Magnetic shielding of nuclei in molecules. Phys Rev. 1950; 78:699–703.
4. Ramsey NF. The internal diamagnetic field correction in measurements of the proton magnetic moment. Phys Rev. 1950; 77:567.
5. Jameson, CJ.; de Dios, AC. Theoretical and physical aspects of nuclear shielding, Nuclear Magnetic Resonance an Specialist Periodical Reports. The Royal Chemical Society; London: 2009. p. 68-93.
6. Vaara J. Theory and computation of nuclear magnetic resonance parameters. Phys Chem Chem Phys. 2007; 9:5399–5418. [PubMed: 17925967]
7. Casabianca LB, de Dios AC. *Ab initio* calculations of NMR chemical shifts. J Chem Phys. 2008; 128:052201–052210. [PubMed: 18266406]
8. Bühl, M.; Graham, AW. Ann Rep on NMR Spectroscopy. Academic Press; 2008. DFT computations of transition-metal chemical shifts; p. 77-126.
9. Kaupp, M.; Bühl, M.; Malkin, V. Theory and Applications. Wiley-VCH; Weinheim: 2004. Calculation of NMR and EPR Parameters.
10. Grant DM, Liu F, Iuliucci RJ, Phung CG, Facelli JC, Alderman DW. Relationship of ^{13}C NMR chemical shift tensors to diffraction structures. Acta Crystal B. 1995; 51:540–546.
11. Iuliucci RJ, Facelli JC, Alderman DW, Grant DM. Carbon-13 chemical shift tensors in polycyclic aromatic compounds. 5. Single-crystal study of acenaphthene. J Am Chem Soc. 1995; 117:2336–2343.
12. Iuliucci, RJ.; Facelli, JC.; Grant, DM. A ^{13}C chemical-shift tensor investigation of polycyclic aromatic hydrocarbon single crystals. Book of Abstracts, 216th ACS National Meeting; Boston. August 23–27, 1998; (COMP-052)
13. Iuliucci RJ, Grant DM. One dimensional chemical shift modulated correlation spectroscopy of single-crystals. Solid State NMR. 1996; 6:55–62.
14. Iuliucci RJ, Phung CG, Facelli JC, Grant DM. Carbon-13 chemical shift tensors in polycyclic aromatic compounds. 6. Single-crystal study of perylene. J Am Chem Soc. 1996; 118:4880–4888.
15. Iuliucci RJ, Phung CG, Facelli JC, Grant DM. Carbon-13 chemical shift tensors in polycyclic aromatic compounds. 7. Symmetry augmented chemical shift-chemical shift correlation spectroscopy and single crystal study of triphenylene. J Am Chem Soc. 1998; 120:9305–9311.
16. Sefzik T, Turco D, Iuliucci RJ, Facelli JC. Modeling NMR chemical shifts: a survey of density functional approaches for calculating tensor properties. J Phys Chem. 2005; 109:1180–1187.
17. Sefzik TH, Fidler JM, Iuliucci R, Facelli JC. Modeling the ^{13}C chemical-shift tensor in organic single-crystals by quantum mechanical methods: finite basis set effects. Magn Reson Chem. 2006; 44:390–400. [PubMed: 16477672]
18. Liu F, Orendt AM, Alderman DW, Grant DM. Carbon-13 chemical shift tensors in pentaerythritol. J Am Chem Soc. 1997; 119:8981–8984.
19. Liu F, Phung CG, Alderman DW, Grant DM. Carbon-13 chemical shift tensors in methyl glycosides, comparing diffraction and optimized structures with single-crystal NMR. J Am Chem Soc. 1996; 118:10629–10634.
20. Liu F, Phung CG, Alderman DW, Grant DM. Analyzing and assigning carbon-13 chemical-shift tensors in fructose, sorbose, and xylose single crystals. J Magn Reson. 1996; 120:231–241.
21. Liu F, Phung CG, Alderman DW, Grant DM. Analyzing and assigning carbon-13 chemical shift tensors in a-L-rhamnose monohydrate single crystals. J Magn Reson. 1996; 120:242–248.

22. Orendt, AM. Chemical shift tensor measurement in solids. In: Grant, DM.; Harris, RK., editors. Encyclopedia of Nuclear Magnetic Resonance. John Wiley & Sons; Chichester: 2003. p. 1282-1296.
23. Facelli JC, Grant DM, Michl J. Carbon-13 shielding tensors: experimental and theoretical determination. Acc Chem Res. 1987; 20:152–158.
24. Harris RK, Becker ED, Cabral de Mendez SM, Granger P, Hoffman RE, Zilm KW. Further conventions for NMR shielding and chemical shifts (IUPAC Recomendation 2008). Pure Appl Chem. 2008; 80:59–84.
25. Flygare WH. Spin–rotation interaction and magnetic shielding in molecules. J Chem Phys. 1964; 41:793–800.
26. Mason, J. Multinuclear NMR. Plenum Press; New York: 1987.
27. Facelli JC, Orendt AM, Grant DM, Michl J. IGLO calculations of the antisymmetric components of nuclear magnetic shielding tensors. Chem Phys Lett. 1984; 112:147–149.
28. Anet FAL, O'Leary DJ. The shielding tensor, part 1: understanding its symmetry properties. Concepts Magn Reson. 1991; 3:193–214.
29. Anet FAL, O'Leary DJ. The shielding, tensor, part 2: understanding the strange effects on relaxation. Concepts Magn Reson. 1992; 4:35–52.
30. Buckingham AD, Malm SM. Asymmetry in the nuclear magnetic shielding tensor. Mol Phys. 1971; 22:1127–1130.
31. Cohen-Tannoudji, C.; Diu, B.; Laloe, F. Quantum Mechanics. Wiley; New York: 2006.
32. Epstein ST. Gauge invariance – a brief review. Isr J Chem. 1980; 19:154–158.
33. Ferraro MB, Herr TE, Lazzeretti P, Malagoli M, Zanasi R. Calculation of molecular magnetic properties within the Landau gauge in hydrogen fluoride, ammonia, and methane molecules. J Chem Phys. 1993; 98:4030–4040.
34. Höller RLH. Coupled-Hartree-Fock calculations of susceptibilities and magnetic shielding constants. I. The first row hydrides lithium hydride, beryllium hydride, borane, methane, ammonia, water, and hydrogen fluoride and the hydrocarbons ethyne, ethene, and ethane. Mol Phys. 1980; 41:1017–1040.
35. Bryce DL, Wasylishen RE. Microwave spectroscopy and nuclear magnetic resonance spectroscopy – what is the connection? Acc Chem Res. 2003; 36:327–334. [PubMed: 12755642]
36. Beeler AJ, Orendt AM, Grant DM, Cutts PW, Michl J, Zilm KW, Downing JW, Facelli JC, Schindler MS, Kutzelnigg W. Low-temperature carbon-13 magnetic resonance in solids. 3. Linear and pseudolinear molecules. J Am Chem Soc. 1984; 106:7672–7676.
37. Aucar GA, Oddershede J. Relativistic theory for indirect nuclear spin–spin couplings within the polarization propagator approach. Int J Quant Chem. 1993; 47:425–435.
38. Aucar GA, Saue T, Visscher L, Jensen HJA. On the origin and contribution of the diamagnetic term in four-component relativistic calculations of magnetic properties. J Chem Phys. 1999; 110:6208–6218.
39. Autschbach, J.; Ziegler, T. Relativistic computation of NMR shieldings and spin–spin coupling constants. In: Grant, DM.; Harris, RK., editors. Encyclopedia of Nuclear Magnetic Resonance Supplementary Volume. John Wiley & Sons; Chichester: 2002. p. 306-323.
40. Melo JI, Ruiz de Azua MC, Giribet CG, Aucar GA, Romero RH. Relativistic effects on the nuclear magnetic shielding tensor. J Chem Phys. 2003; 118:471–486.
41. Pyykko P, Wiesenfeld L. Relativistically parameterized extended Hueckel calculations. IV. Nuclear spin–spin coupling tensors for main group elements. Mol Phys. 1981; 43:557–580.
42. Visscher L, Enevoldsen T, Saue T, Jensen HJA, Oddershede J. Full four-component relativistic calculations of NMR shielding and indirect spin–spin coupling tensors in hydrogen halides. J Comput Chem. 1999; 20:1262–1273.
43. Yates JR, Pickard CJ, Payne MC, Mauri F. Relativistic nuclear magnetic resonance chemical shifts of heavy nuclei with pseudopotentials and the zeroth-order regular approximation. J Chem Phys. 2003; 118:5746–5753.

44. Cheng L, Xiao YL, Liu WJ. Four-component relativistic theory for NMR parameters: unified formulation and numerical assessment of different approaches. J Chem Phys. 2009; 130:144102–144118. [PubMed: 19368424]
45. Liu WJ, Peng DL. Exact two-component Hamiltonians revisited. J Chem Phys. 2009; 131:031104. [PubMed: 19624172]
46. Xiao YL, Liu WJ, Cheng L, Peng DL. Four-component relativistic theory for nuclear magnetic shielding constants: critical assessments of different approaches. J Chem Phys. 2007; 126:214101–214111. [PubMed: 17567184]
47. Komorovsky S, Repisky M, Malkina OL, Malkin VG, Ondik IM, Kaupp M. A fully relativistic method for calculation of nuclear magnetic shielding tensors with a restricted magnetically balanced basis in the framework of the matrix Dirac–Kohn–Sham equation. J Chem Phys. 2008; 128:104101–104115. [PubMed: 18345871]
48. Wolff SK, Ziegler T, van Lenthe E, Baerends EJ. Density functional calculations of nuclear magnetic shieldings using the zeroth-order regular approximation (ZORA) for relativistic effects: ZORA nuclear magnetic resonance. J Chem Phys. 1999; 110:7689–7698.
49. Velde GT, Bickelhaupt FM, Baerends EJ, Guerra CF, Van Gisbergen SJA, Snijders JG, Ziegler T. Chemistry with ADF. J Comput Chem. 2001; 22:931–967.
50. Fukui H, Baba T. Calculation of nuclear magnetic shieldings. XV. *Ab initio* zeroth-order regular approximation method. J Chem Phys. 2002; 117:7836–7844.
51. Schreckenbach G. NMR shielding calculations across the periodic table: diamagnetic uranium compounds. 2. Ligand and metal NMR. Inorg Chem. 2002; 41:6560–6572. [PubMed: 12470051]
52. Bagno A, Bonchio M. Relativistic DFT calculation of Ru-99 NMR parameters: chemical shirts and spin–spin coupling constants. Magn Reson Chem. 2004; 42:S79–S87. [PubMed: 15366044]
53. Bagno A, Bonchio M, Autschbach J. Computational modeling of polyoxotungstates by relativistic DFT calculations of W-183 NMR chemical shifts. Chem Eur J. 2006; 12:8460–8471. [PubMed: 16927351]
54. Bagno A, Casella G, Saielli G. Relativistic DFT calculation of Sn-119 chemical shifts and coupling constants in tin compounds. J Chem Theory Comput. 2006; 2:37–46.
55. Chierotti MR, Garlaschelli L, Gobetto R, Nervi C, Peli G, Sironi A, Della Pergola R. An unusual carbonyl chemical shift in a carbonylhexairidium cluster: a combined solid-state NMR and DFT approach. Eur J Inorg Chem. 2007:3477–3483.
56. Demko BA, Eichele K, Wasylishen RE. A combined experimental and quantum chemistry study of selenium chemical shift tensors. J Phys Chem A. 2006; 110:13537–13550. [PubMed: 17165881]
57. Dmitrenko O, Bai S, Dybowski C. Prediction of Pb-207 NMR parameters for the solid ionic lead(II) halides using the relativistic ZORA-DFT formalism: comparison with the lead-containing molecular systems. Solid State NMR. 2008; 34:186–190.
58. Forgeron MAM, Wasylishen RE. A solid-state Mo-95 NMR and computational investigation of dodecahedral and square antiprismatic octacyanomolybdate(IV) anions: is the point-charge approximation an accurate probe of local symmetry? J Am Chem Soc. 2006; 128:7817–7827. [PubMed: 16771495]
59. Fowe EP, Belser P, Daul C, Chermette H. Assessment of theoretical prediction of the NMR shielding tensor of (PtClxBr6-x2-)-Pt-195 complexes by DFT calculations: experimental and computational results. Phys Chem Chem Phys. 2005; 7:1732–1738. [PubMed: 19787932]
60. Gracia J, Poblet JM, Autschbach J, Kazansky LP. Density-functional calculation of the W-183 and O-17 NMR chemical shifts for large polyoxotungstates. Eur J Inorg Chem. 2006:1139–1148.
61. Krykunov M, Ziegler T, van Lenthe E. Implementation of a hybrid DFT method for calculating NMR shieldings using slater-type orbitals with spin–orbital coupling included. Applications to (OS)-O-187, Pt-195, and C-13 in heavy-metal complexes. J Phys Chem A. 2009; 113:11495–11500. [PubMed: 19731903]
62. Nahrwold S, Berger R. Zeroth order regular approximation approach to parity violating nuclear magnetic resonance shielding tensors. J Chem Phys. 2009; 130:214101–214114. [PubMed: 19508050]

63. Neto AC, Ducati LC, Rittner R, Tormena CF, Contreras RH, Frenking G. Heavy halogen atom effect on C-13 NMR chemical shifts in monohalo derivatives of cyclohexane and pyran. Experimental and theoretical study. J Chem Theory Comput. 2009; 5:2222–2228.
64. Orian L, Bisello A, Santi S, Ceccon A, Saielli G. Rh-103 NMR chemical shifts in organometallic complexes: a combined experimental and density functional study. Chem Eur J. 2004; 10:4029–4040. [PubMed: 15316995]
65. Straka M, Kaupp M. Calculation of F-19 NMR chemical shifts in uranium complexes using density functional theory and pseudopotentials. Chem Phys. 2005; 311:45–56.
66. Taylor RE, Carver CT, Larsen RE, Dmitrenko O, Bai S, Dybowski C. Revisiting $HgCl_2$: a solution and solid-state Hg-199 NMR and ZORA-DFT computational study. J Mol Struct. 2009; 930:99–109.
67. Willans MJ, Feindel KW, Ooms KJ, Wasylishen RE. An investigation of lanthanum coordination compounds by using solid-state La-139 NMR spectroscopy and relativistic density functional theory. Chem Eur J. 2006; 12:159–168. [PubMed: 16224769]
68. Wren JEC, Schreckenbach G. Neptunium(VII) in high-ionic-strength alkaline solutions – [NpO2(OH)(4)](1-) or [NpO4(OH)(2)](3-)? Canad J Chem. 2009; 87:1436–1443.
69. Chesnut DB. Some recent *ab initio* calculations of NMR chemical shifts. Ann Rep NMR Spectrosc. 1989; 21:51–97.
70. Chesnut DB. Ab initio calculations of NMR chemical shielding. Ann Rep NMR Spectrosc. 1994; 29:71–122.
71. de Dios AC, Jameson CJ. The NMR chemical shifts: insight into structure and environment. Ann Rep NMR Spectrosc. 1994; 29:1–69.
72. Jameson, CJ.; de Dios, AC. Specialist Periodical Reports on Nuclesar Magnetic Resonance. Vol. 28. The Royal Chemical Society; London: 1999. Theoretical and physical aspects of nuclear shielding; p. 42-76.
73. de Dios AC, Oldfield E. Recent progress in understanding chemical shifts. Solid State NMR. 1996; 6:101–125.
74. Fleicher, U.; van Wüllen, C.; Kutzelnigg, W. NMR chemical shift computation: ab initio. In: von RaguéSchleyer, P., editor. Encyclopedia of Computational Chemistry. John Wiley & Sons; Chichester: 1998. p. 1827-1835.
75. Kutzelnigg, W.; Fleischer, U.; van Wüllen, C. Shielding calculations: IGLO method. In: Grant, DM.; Harris, RK., editors. Encyclopedia of Nuclear Magnetic Resonance. John Wiley & Sons; Chichester: 1996. p. 4284-4291.
76. Kutzelnigg W, Fleischer U, Schindler M. The IGLO-method: *ab initio* calculation and interpretation of NMR chemical shifts and magnetic susceptibilities. NMR Basic Princ Prog. 1990; 23:165–262.
77. Vaara J, Jokisaari J, Wasylishen RE, Bryce DL. Spin–spin coupling tensors as determined by experiment and computational chemistry. Prog NMR Spectrosc. 2002; 41:233–304.
78. Pickard, CJ.; Mauri, F. Calculation of magnetic resonance parameters in solids and liquids using periodic boundary conditions. In: Kaupp, M.; Bühl, M.; Malkin, VG., editors. Calculation of NMR and EPR Parameters. Wiley VCH Verlag GmbH & Co; KGaA, Weinheim: 2004.
79. Facelli JC, Grant DM. Determination of molecular symmetry in crystalline naphthalene using solid-state NMR. Nature (London). 1993; 365:325–327. [PubMed: 8377823]
80. Harris, RK.; Wasylishen, RE.; Duer, MJ. NMR Crystallography. Wiley; 2009.
81. Brouwer DH. A structure refinement strategy for NMR crystallography: an improved crystal structure of silica-ZSM-12 zeolite from Si-29 chemical shift tensors. J Magn Reson. 2008; 194:136–146. [PubMed: 18656402]
82. Brouwer DH, Alavi S, Ripmeester JA. NMR crystallography of *p*-tert-butylcalix[4] arene host–guest complexes using H-1 complexation-induced chemical shifts. Phys Chem Chem Phys. 2008; 10:3857–3860. [PubMed: 18688383]
83. Grant DM, Halling MD. Metric spaces in NMR crystallography. Concepts Magn Reson. 2009; 34A:217–237.
84. Harris RK. NMR crystallography: the use of chemical shifts. Solid State Sci. 2004; 6:1025–1037.

85. Harris RK. NMR studies of organic polymorphs & solvates. Analyst. 2006; 131:351–373. [PubMed: 16496044]

86. Harris RK, Hodgkinson P, Pickard CJ, Yates JR, Zorin V. Chemical shift computations on a crystallographic basis: some reflections and comments. Magn Reson Chem. 2007; 45:S174–S186. [PubMed: 18157842]

87. Marek R, Lycka A, Kolehmainen E, Sievanen E, Tousek J. N-15 NMR spectroscopy in structural analysis: an update (2001–2005). Curr Org Chem. 2007; 11:1154–1205.

88. Pickard CJ, Salager E, Pintacuda G, Elena B, Emsley L. Resolving structures from powders by NMR crystallography using combined proton spin diffusion and plane wave DFT calculations. J Am Chem Soc. 2007; 129:8932–8933. [PubMed: 17602560]

89. Salager E, Stein RS, Pickard CJ, Elena B, Emsley L. Powder NMR crystallography of thymol. Phys Chem Chem Phys. 2009; 11:2610–2621. [PubMed: 19421517]

90. Bertini, I.; Luchinat, C.; Parigu, G. Solution NMR of Paramagnetic Molecules. Elsevier; Amsterdam: 2001.

91. Ando I, Webb GA. Some quantum chemical aspects of solvent effects on NMR parameters. Org Magn Reson. 1981; 15:111–130.

92. Ando, I.; Webb, GA. Theory of NMR Parameters. Academic Press; London: 1983.

93. Webb, GA. Shielding: overview of theoretical methods. In: Grant, DM.; Harris, RK., editors. Encyclopedia of Nuclear Magnetic Resonance. John Wiley & Sons; Chichester: 1996. p. 4307-4318.

94. Williams DE, Peters MB, Wang B, Roitberg AE, Merz KM. AM1 parameters for the prediction of H-1 and C-13 NMR chemical shifts in proteins. J Phys Chem A. 2009; 113:11550–11559. [PubMed: 19799435]

95. Williams DE, Peters MB, Wang B, Merz KM. MNDO parameters for the prediction of F-19 NMR chemical shifts in biologically relevant compounds. J Phys Chem A. 2008; 112:8829–8838. [PubMed: 18722416]

96. Patchkovskii S, Thiel W. NMR chemical shifts in MNDO approximation: parameters and results for H, C, N, and O. J Comput Chem. 1999; 20:1220–1245.

97. Sitkoff D, Case DA. Theories of chemical shift anisotropies in proteins and nucleic acids. Prog NMR Spectrosc. 1998; 32:165–190.

98. Sternberg, U.; Witter, R.; Ulrich, AS. Advances in Solid State NMR Studies of Materials and Polymers: A Special Volume Dedicated to Isao Ando. Academic Press Ltd; London: 2004. 3D structure elucidation using NMR chemical shifts; p. 53-104.

99. Blinov KA, Smurnyy YD, Churanova TS, Elyashberg ME, Williams AJ. Development of a fast and accurate method of ^{13}C NMR chemical shift prediction. Chemomet Intell Lab Syst. 2009; 97:91–97.

100. Shen Y, Delaglio F, Cornilescu G, Bax A. TALOS plus: a hybrid method for predicting protein backbone torsion angles from NMR chemical shifts. J Biomol NMR. 2009; 44:213–223. [PubMed: 19548092]

101. Shen Y, Bax A. Protein backbone chemical shifts predicted from searching a database for torsion angle and sequence homology. J Biomol NMR. 2007; 38:289–302. [PubMed: 17610132]

102. Cornilescu G, Delaglio F, Bax A. Protein backbone angle restraints from searching a database for chemical shift and sequence homology. J Biomol NMR. 1999; 13:289–302. [PubMed: 10212987]

103. Szabo, A.; Ostlund, NS. Modern Quantum Chemistry. McGraw-Hill; New York: 1982.

104. Pople JA. Molecular orbital theory of diamagnetism. I. An approximate L.C.A.O. scheme. J Chem Phys. 1962; 36:53–59.

105. Contreras RH, Facelli JC. Advances in theoretical and physical aspects of spin–spin coupling constants. Ann Rep NMR Spectrosc. 1993; 27:255–356.

106. Christian Ochsenfeld JKFK. *Ab initio* nmr spectra for molecular systems with a thousand and more atoms: a linear-scaling methods. Angew Chem, Int Ed. 2004; 43:4485–4489.

107. Kussmann J, Ochsenfeld C. A density matrix-based method for the linear-scaling calculation of dynamic second- and third-order properties at the Hartree-Fock and Kohn–Sham density functional theory levels. J Chem Phys. 2007:127.

108. Grant DM, Facelli JC, Alderman DW, Sherwood MH. Carbon-13 chemical shielding tensors in sugars: sucrose and methyl a-D-glucopyranoside, NATO ASI Ser. Ser C: Math Phys Sci. 1993; 386:367–384.
109. Sauer, SPA.; Oddershede, J. Correlated and gauge invariant calculations of nuclear shielding constants. In: Tossel, JA., editor. Nuclear Magnetic Shielding and Structure. Kluwer; Dordrecht: 1993. p. 351-365.
110. Gauss, J.; Stanton, JF. Electron-correlated approaches for the calculation of NMR chemical shifts. In: Prigogine, I.; Rice, SA., editors. Advances in Chemical Physics. John Wiley & Sons; 2002. p. 366-422.
111. Seminario JM. An introduction to density functional theory in chemistry. Theor Comput Chem. 1995; 2:1–27.
112. Beer M, Ochsenfeld C. Efficient linear-scaling calculation of response properties: density matrix-based Laplace-transformed coupled-perturbed self-consistent field theory. J Chem Phys. 2008; 128
113. Schreckenbach G. On the relation between a common gauge origin formulation and the GIAO formulation of the NMR shielding tensor. Theor Chim Acta. 2002; 108:246–253.
114. Wilson PJ, Amos RD, Handy NC. Density functional predictions for magnetizabilities and nuclear shielding constants. Mol Phys. 1999; 97:757–768.
115. Cheeseman JR, Trucks GW, Keith TA, Frisch MJ. A comparison of models for calculating nuclear magnetic resonance shielding tensors. J Chem Phys. 1996; 104:5497–5509.
116. Wiberg KB, Hammer JD, Zilm KW, Keith TA, Cheeseman JR, Duchamp JC. NMR chemical shifts substituted acetylenes. J Org Chem. 2004; 69:1086–1096. [PubMed: 14961656]
117. Perdew JP, Tao JM, Staroverov VN, Scuseria GE. Meta-generalized gradient approximation: explanation of a realistic nonempirical density functional. J Chem Phys. 2004; 120:6898–6911. [PubMed: 15267588]
118. Perdew JP, Ruzsinszky A, Tao JM, Staroverov VN, Scuseria GE, Csonka GI. Prescription for the design and selection of density functional approximations: more constraint satisfaction with fewer fits. J Chem Phys. 2005; 123:62201–62209. [PubMed: 16122287]
119. Janesko BG, Henderson TM, Scuseria GE. Screened hybrid density functionals for solid-state chemistry and physics. Phys Chem Chem Phys. 2009; 11:443–454. [PubMed: 19283261]
120. Keal TW, Tozer DJ, Helgaker T. GIAO shielding constants and indirect spin– spin coupling constants: performance of density functional methods. Chem Phys Lett. 2004; 391:374–379.
121. Keal TW, Tozer DJ. A semiempirical generalized gradient approximation exchange-correlation functional. J Chem Phys. 2004; 121:5654–5660. [PubMed: 15366989]
122. Keal TW, Tozer DJ. The exchange-correlation potential in Kohn–Sham nuclear magnetic resonance shielding calculations. J Chem Phys. 2003; 119:3015–3024.
123. Allen MJ, Keal TW, Tozer DJ. Improved NMR chemical shifts in density functional theory. Chem Phys Lett. 2003; 380:70–77.
124. Epstein ST. Ehrenfest's theorem and the (generalized) TRK [Thomas–Reiche–Kuhn] sum rule for variational wave functions. J Chem Phys. 1973; 58:5184–5185.
125. Grant DM, Facelli JC, Alderman DW, Sherwood MH. Carbon-13 chemical shielding tensors in sugars: sucrose and methyl a-D-glucopyranoside, NATO ASI Ser. Ser C: Math Phys Sci. 1993; 386:367–384.
126. Facelli JC, Grant DM, Michl J. Analysis of the IGLO bond contributions to the carbon-13 shielding tensors in the local bond frame. Int J Quant Chem. 1987; 31:45–55.
127. Facelli JC, Grant DM, Bouman TD, Hansen AE. A comparison of the IGLO and LORG methods for the calculation of nuclear magnetic shieldings. J Comput Chem. 1990; 11:32–44.
128. Hansen, AE.; Bilde, M. Shielding calculations: LORG and SOLO approaches. In: Grant, DM.; Harris, RK., editors. Encyclopedia of Nuclear Magnetic Resonance. John Wiley & Sons; Chichester: 1996. p. 4292-4299.
129. Keith TA, Bader RFW. Calculation of magnetic response properties using atoms in molecules. Chem Phys Lett. 1992; 194:1–8.

130. Keith TA, Bader RFW. Calculation of magnetic response properties using a continuous set of gauge transformations. Chem Phys Lett. 1993; 210:223–231.
131. Geertsen J. A solution of the gauge-origin problem for the magnetic shielding constant. Chem Phys Lett. 1991; 179:479–482.
132. Bader, RFW. Atoms in Molecules – A Quantum Theory. Oxford University Press; Oxford: 1990.
133. Dunning TH Jr. Gaussian basis sets for use in correlated molecular calculations. I. The atoms boron through neon and hydrogen. J Chem Phys. 1989; 90:1007–1023.
134. Hehre WJ, Stewart RF, Pople JA. Self-consistent molecular-orbital methods. I. Use of Gaussian expansions of Slater-type atomic orbitals. J Chem Phys. 1969; 51:2657–2664.
135. Facelli JC. Calculation of chemical shieldings: theory and application. Concepts Magn Reson. 2004; 20A:42–69.
136. Jameson CJ, Jameson AK, Parker H, Cohen SM, Lee C-L. Variation of chemical shielding with intermolecular interactions and rovibrational motion. II. Nitrogen-15 and carbon-13 nuclei in nitrous oxide and carbon dioxide. J Chem Phys. 1978; 68:2861–2867.
137. Jameson AK, Jameson CJ. Gas-phase carbon-13 chemical shifts in the zero-pressure limit: refinements to the absolute shielding scale for carbon-13. Chem Phys Lett. 1987; 134:461–466.
138. Wasylishen RE, Friedrich JO. Deuterium isotope effects on nuclear shielding constants and spin–spin coupling constants in the ammonium ion, ammonia, and water. Canad J Chem. 1987; 65:2238–2243.
139. Jameson, CJ. Isotope effects on chemical shifts and coupling constants. In: Grant, DM.; Harris, RK., editors. Encyclopedia of Magnetic Resonance. John Wiley & Sons; Chichester: 1996.
140. Buckingham AD. Chemical shift in the nuclear magnetic resonance spectra of molecules containing polar groups. Canad J Chem. 1960; 38:300–307.
141. Buckingham AD, Schaefer T, Scheneider WC. Solvent effects in nuclear magnetic resonance spectra. J Chem Phys. 1960; 32:1227–1234.
142. Rummens FHA. NMR Basic Princ Prog. 1975; 10:1.
143. de Dios AC. *Ab initio* calculations of the NMR chemical shift. Prog Nucl Magn Reson. 1996; 29:229.
144. Bagno A, Rastrelli F, Saielli G. NMR techniques for the investigation of solvation phenomena and non-covalent interactions. Prog Nucl Magn Reson Spectrosc. 2005; 47:41–93.
145. Germer HA. Solvent interaction within the Hartree-Fock SCF molecular orbital formalism. Theor Chim Acta. 1974; 34:145–155.
146. de Dios AC, Pearson JG, Oldfield E. *Secondary and tertiary structural effects on protein NMR chemical shifts: an, ab initio* approach, Science (Washington. DC. United States). 1993; 260:1491–1496.
147. Hehre WJ, Stewart RF, Pople JA. Self-consistent molecular-orbital methods. I. Use of Gaussian expansions of Slater-type atomic orbitals. J Chem Phys. 1969; 51:2657–2664.
148. Orendt AM, Facelli JC. Solid state effects on NMR chemical shifts. Ann Rep NMR Spectrosc. 2007; 62:115–178.
149. Augspurger, JD.; Dykstra, CE.; Oldfield, E.; Pearson, JG. Nuclear Quadrupole Resonance and Infra-red Spectroscopic Parameters from *Ab initio* Calculation and Experiment: From CO to Proteins. Kluwer Academic Publisher; Boston: 1993. Intra- and Intermolecular Electrical Effects on Nuclear Magnetic Resonance.
150. de Dios AC, Oldfield E. Methods for computing nuclear magnetic resonance chemical shielding in large systems. Multiple cluster and charge field approaches. Chem Phys Lett. 1993; 205:108–116.
151. Stueber D, Guenneau FN, Grant DM. The calculation of ^{13}C chemical shielding tensors in ionic compounds utilizing point charge arrays obtained from Ewald lattice sums. J Chem Phys. 2001; 114:9236–9243.
152. Stueber D, Orendt AM, Facelli JC, Parry RW, Grant DM. Carbonates, thiocarbonates, and the corresponding monoalkyl derivatives. III. The ^{13}C chemical shift tensors in potassium carbonate, bicarbonate and related monomethyl derivatives. Solid State NMR. 2002; 22:29–49.

153. Solis D, Ferraro MB, Facelli JC. Modeling NMR chemical shifts: surface charge representation of the electrostatic embedding potential modeling of crystalline intermolecular effects in 19F solid state NMR chemical shifts. J Mol Struct. 2002:602–603. 159–164.

154. Solis D, Ferraro MB. Solid-state nuclear magnetic resonance: performance of point-charge distributions to model intermolecular effects in ^{19}F chemical shifts. Theor Chem Accounts. 2000; 104:323–326.

155. Ferraro MB, Repetto V, Facelli JC. Modeling NMR chemical s: a comparison of charge models for solid state effects on ^{15}N chemical shift tensors. Solid State NMR. 1998; 10:185–189.

156. Di Fiori N, Orendt AM, Caputo MC, Ferraro MB, Facelli JC. Modeling solid state effects on NMR chemical shifts using electrostatic models. Magn Reson Chem. 2004; 42:S41–S47. [PubMed: 15366040]

157. Ma Z, Halling MD, Solum MS, Harper JK, Orendt AM, Facelli JC, Pugmire RJ, Grant DM, Amick AW, Scott LT. Ring current effects in a crystal. Evidence from ^{13}C chemical shielding tensors for intermolecular shielding and molecular magnetic susceptibility in 4,7-di-t-butylacenaphthene versus 4,7-di-t-butylacenaphthylene. J Phys Chem A. 2007; 111:2020–2027. [PubMed: 17388281]

158. Jiao H, Schleyer PvR, Beno BR, Houk KN, Warmuth R. Theoretical studies of the structure, aromaticity, and magnetic properties of o-benzyne. Angew Chem, Int Ed. 1998; 36:2761–2764.

159. Jemmis ED, Subramanian AJ, Kos P, von Ragué Schleyer P. The remarkably stabilized trilithiocyclopropenium ion, C3Li3+, and its relatives. J Am Chem Soc. 1997; 119:9504–9512.

160. von RaguéSchleyer P, Maerker C, Dransfeld H, Jiao H, van Eikema Hommes NJR. Nucleus-independent chemical shifts: a simple and efficient aromaticity probe. J Am Chem Soc. 1996; 118:6317–6318.

161. Facelli JC. Intermolecular shielding by molecular magnetic susceptibility. A new view of intermolecular ring current effects. Magn Reson Chem. 2006; 44:401–408. [PubMed: 16477673]

162. Sebastiani D. Ab-initio calculations of nmr parameters in condensed phases. Modern Phys Lett B. 2003; 17:1301–1319.

163. Sebastiani D. Current densities and nucleus-independent chemical shift maps from reciprocal-space density functional perturbation theory calculations. Chem Phys Phys Chem. 2006; 7:164–175.

164. Sebastiani D, Goward G, Schnell I, Parrinello M. NMR chemical shifts in periodic systems from first principles. Comput Phys Commun. 2002; 147:707–710.

165. Sebastiani D, Goward G, Schnell I, Spiess HW. NMR chemical shifts in proton conduction crystals from first principles. J Mol Struct (Theochem). 2003; 625:283–288.

166. Sebastiani D, Parrinello M. A new ab-initio approach for the calculation of NMR chemical shifts in periodic systems. J Phys Chem A. 2001; 105:1951–1958.

167. Sebastiani D, Rothlisberger U. Nuclear magnetic resonance chemical shifts from hybrid DFT QM/MM calculations. J Phys Chem B. 2004; 108:2807–2815.

168. Parrinello M, Andreoni W. CPMD V39 Copyright IBM Corp. 1990–2006, Copyright MPI fuer Festkoerperforschung Stuttgart, 1997–2001. <http://www.cpmd.org/>

169. Mauri F, Pfrommer BG, Louie SG. *Ab initio* theory of NMR chemical shifts in solids and liquids. Phys Rev Lett. 1996; 77:5300–5303. [PubMed: 10062766]

170. Pickard CJ, Mauri F. All-electron magnetic response with pseudopotentials: NMR chemical shifts. Phys Rev B. 2001; 63:245101.

171. Benoit M, Profeta M, Mauri F, Pickard CJ, Tuckerman ME. First-principles calculation of the ^{17}O NMR parameters of a calcium aluminosilicate glass. J Phys Chem B. 2005; 109:6052–6060. [PubMed: 16851665]

172. Buda F, Giannozzi P, Mauri F. Density functional theory study of the structure and ^{13}C chemical shifts of retinylidene iminium salts. J Phys Chem B. 2000; 104:9048–9053.

173. Gervais C, Profeta M, Babonneau F, Pickard CJ, Mauri F. *Ab initio* calculations of NMR parameters of highly coordinated oxygen sites in aluminosilicates. J Phys Chem B. 2004; 108:13249–13253.

174. Gervais C, Profeta M, Lafond V, Bonhomme C, Azais T, Mutin H, Pickard CJ, Mauri F, Babonneau F. Combined *ab initio* computational and experimental multinuclear solid-state

magnetic resonance study of phenylphosphonic acid. Magn Reson Chem. 2004; 42:445–452. [PubMed: 15095380]

175. Gregor T, Mauri F, Car R. A comparison of methods for the calculation of NMR chemical shifts. J Chem Phys. 1999; 111:1815–1822.
176. Pfrommer BG, Mauri F, Louie SG. NMR chemical shifts of ice and liquid water: the effects of condensation. J Am Chem Soc. 2000; 122:123–129.
177. Profeta M, Benoit M, Mauri F, Pickard CJ. First-principles calculation of the ^{17}O NMR parameters in Ca oxide and Ca aluminosilicates: the partially covalent nature of the Ca–O Bond, a challenge for density functional theory. J Am Chem Soc. 2004; 126:12628–12635. [PubMed: 15453796]
178. Rossano S, Mauri F, Pickard CJ, Farnan I. First-principles calculation of ^{17}O and ^{25}Mg NMR shieldings in MgO at finite temperature: rovibrational effect in solids. J Phys Chem B. 2005; 109:7245–7250. [PubMed: 16851828]
179. Yates JR, Dobbins SE, Pickard CJ, Mauri F, Ghi PY, Harris RK. A combined first principles computational and solid state NMR study of a molecular crystal: flurbiprofen. Phys Chem Chem Phys. 2005; 7:1402–1407. [PubMed: 19787961]
180. Yates JR, Pickard CJ, Payne MC, Dupree R, Profeta M, Mauri F. Theoretical investigation of oxygen-17 NMR shielding and electric field gradients in glutamic acid polymorphs. J Phys Chem A. 2004; 108:6032–6037.
181. Giannozzi P, Baroni S, Bonini N, Calandra M, Car R, Cavazzoni C, Ceresoli D, Chiarotti GL, Cococcioni M, Dabo I, Corso AD, Gironcoli SD, Fabris S, Fratesi G, Gebauer R, Gerstmann U, Gougoussis C, Kokalj A, Lazzeri M, Martin-Samos L, Marzari N, Mauri F, Mazzarello R, Paolini S, Pasquarello A, Paulatto L, Sbraccia C, Scandolo S, Sclauzero G, Seitsonen AP, Smogunov A, Umari P, Wentzcovitc RM. QUANTUM ESPRESSO: a modular and open-source software project for quantum simulations of materials. J Phys: Condens Matter. 2009; 21:395502–395519. [PubMed: 21832390]
182. Frisch, MJ.; Trucks, GW.; Schlegel, HB.; Scuseria, GE.; Robb, MA.; Cheeseman, JR.; Scalmani, G.; Barone, V.; Mennucci, B.; Petersson, GA.; Nakatsuji, H.; Caricato, M.; Li, X.; Hratchian, HP.; Izmaylov, AF.; Bloino, J.; Zheng, G.; Sonnenberg, JL.; Hada, M.; Ehara, M.; Toyota, K.; Fukuda, R.; Hasegawa, J.; Ishida, M.; Nakajima, T.; Honda, Y.; Kitao, O.; Nakai, H.; Vreven, T.; Montgomery, JJA.; Peralta, JE.; Ogliaro, F.; Bearpark, M.; Heyd, JJ.; Brothers, E.; Kudin, KN.; Staroverov, VN.; Kobayashi, R.; Normand, J.; Raghavachari, K.; Rendell, A.; Burant, JC.; Iyengar, SS.; Tomasi, J.; Cossi, M.; Rega, N.; Millam, JM.; Klene, M.; Knox, JE.; Cross, JB.; Bakken, V.; Adamo, C.; Jaramillo, J.; Gomperts, R.; Stratmann, RE.; Yazyev, O.; Austin, AJ.; Cammi, R.; Pomelli, C.; Ochterski, JW.; Martin, RL.; Morokuma, K.; Zakrzewski, VG.; Voth, GA.; Salvador, P.; Dannenberg, JJ.; Dapprich, S.; Daniels, AD.; Farkas, Ö.; Foresman, JB.; Ortiz, JV.; Cioslowski, J.; Fox, DJ. Gaussian 09, Revision A1. Gaussian, Inc; Wallingford, CT: 2010.
183. Pulay, P.; Hinton, JF. Shielding theory: GIAO method. In: Grant, DM.; Harris, RK., editors. Encyclopedia of Nuclear Magnetic Resonance. John Wiley & Sons; Chichester: 1996. p. 4334-4339.
184. Wolinski K, Hinton JF, Pulay P. Efficient implementation of the gauge-independent atomic orbital method for NMR chemical shift calculations. J Am Chem Soc. 1990; 112:8251–8260.
185. Malkin VG, Malkina OL, Casida ME, Salahub DR. Nuclear magnetic resonance shielding tensors calculated with a sum-over-states density functional perturbation theory. J Am Chem Soc. 1994; 116:5898–5908.
186. Becke AD. Density-functional thermochemistry. III. The role of exact exchange. J Chem Phys. 1993; 98:5648–5652.
187. Adamo C, Barone V. Toward reliable adiabatic connection models free from adjustable parameters. Chem Phys Lett. 1997; 274:242–250.
188. Handy NC, Cohen AJ. Left-right correlation energy. Mol Phys. 2001; 99:403–412.
189. Curtiss LA, Raghavachari K, Redfern PC, Rassolov V, Pople JA. Gaussian-3 theory for molecular energies of first- and second-row compound. J Chem Phys. 1998; 109:7764–7777.

190. Curtiss LA, Raghavachari K, Trucks GW, Pople JA. Gaussian-2 theory for molecular energies of first- and second-row compounds. J Chem Phys. 1991; 94:7221–7231.

191. Facelli, JC. Modeling NMR chemical shifts. In: Webb, GA., editor. Modern Magnetic Resonance. Springer; 2006. p. 49-58.

192. Frisch, MJ.; Trucks, GW.; Schlegel, HB.; Cuseria, GE.; Robb, MA.; Cheeseman, JR.; Montgomery, JA., Jr; Vreven, T.; Kudin, KN.; Burant, JC.; Millam, JM.; Iyengar, SS.; Tomasi, J.; Barone, V.; Mennucci, B.; Cossi, M.; Scalmani, G.; Rega, N.; Petersson, GA.; Nakatsuji, H.; Hada, M.; Ehara, M.; Toyota, K.; Fukuda, R.; Hasegawa, J.; Ishida, M.; Nakajima, T.; Honda, Y.; Kitao, O.; Nakai, H.; Klene, M.; Li, X.; Knox, JE.; Hratchian, HP.; Cross, JB.; Bakken, V.; Adamo, C.; Jaramillo, J.; Gomperts, R.; Stratmann, RE.; Yazyev, O.; Austin, AJ.; Cammi, R.; Pomelli, C.; Ochterski, JW.; Ayala, PY.; Morokuma, K.; Voth, GA.; Salvador, P.; Dannenberg, JJ.; Zakrzewski, VG.; Dapprich, S.; Daniels, AD.; Strain, MC.; Farkas, O.; Malick, DK.; Rabuck, AD.; Raghavachari, K.; Foresman, JB.; Ortiz, JV.; Cui, Q.; Baboul, AG.; Clifford, S.; Cioslowski, J.; Stefanov, BB.; Liu, G.; Liashenko, A.; Piskorz, P.; Komaromi, I.; Martin, RL.; Fox, DJ.; Keith, T.; Al-Laham, MA.; Peng, CY.; Nanayakkara, A.; Challacombe, M.; Gill, PMW.; Johnson, B.; Chen, W.; Wong, MW.; Gonzalez, C.; Pople, JA. Gaussian 03, Revision C02. Gaussian, Inc; Wallingford, CT: 2003–2004.

193. Boykin, DW. ^{17}O NMR Spectroscopy in Organic Chemistry. CRC Press; 1990.

194. Alderman DW, Sherwood MH, Grant DM. Comparing, modeling, and assigning chemical-shift tensors in the cartestian, irreducible spherical, and icosahedral representations. J Magn Reson. 1993; 101:188–197.

195. Wang B, Dossey AT, Walse SS, Edison AS, Merz KM. Relative configuration of natural products using NMR chemical shifts. J Nat Prod. 2009; 72:709–713. [PubMed: 19265431]

196. Belostotskii AM. Calculated chemical shifts as a fine tool of conformational analysis: an unambiguous solution for haouamine alkaloids. J Org Chem. 2008; 73:5723–5731. [PubMed: 18597531]

197. Härtner J, Reinscheid UM. Conformational analysis of menthol diastereomers by NMR and DFT computation. J Mol Struct. 2008; 872:145–149.

198. Potrzebowski, M. Organic & pharmaceutical chemistry. In: Harris, RK.; Wasylishen, RE.; Duer, MJ., editors. NMR Crystallography. Wiley; 2009. p. 435-451.

199. Zienau J, Kussmann J, Koziol F, Ochsenfeld C. Molecular recognition in molecular tweezers systems: quantum-chemical calculation of NMR chemical shifts. Phys Chem Chem Phys. 2007; 9:4552–4562. [PubMed: 17690781]

200. Souma H, Shoji A, Kurosu H. Conformational analysis of [alpha]-helical polypeptide included l-proline residue by high-resolution solid-state NMR measurement and quantum chemical calculation. J Mol Struct. 2008; 889:237–243.

201. Vila JA, Aramini JM, Rossi P, Kuzin A, Su M, Seetharaman J, Xiao R, Tong L, Montelione GT, Scheraga HA. Quantum chemical ^{13}C chemical shift calculations for protein NMR structure determination, refinement, and validation. Proc Natl Acad Sci. 2008; 105:14389–14394. [PubMed: 18787110]

202. Vila JA, Ripoll DR, Scheraga HA. Use of 13C-a chemical shifts in protein structure determination. J Phys Chem B. 2007; 111:6577–6585. [PubMed: 17516673]

203. Vila JA, Villegas ME, Baldoni HA, Scheraga HA. Predicting C-13(alpha) chemical shifts for validation of protein structures. J Biomol NMR. 2007; 38:221–235. [PubMed: 17558470]

204. Gao Q, Yokojima S, Kohno T, Ishida T, Fedorov DG, Kitaura K, Fujihira M, Nakamura S. *Ab initio* NMR chemical shift calculations on proteins using fragment molecular orbitals with electrostatic environment. Chem Phys Lett. 2007; 445:331–339.

205. He X, Wang B, Merz KM. Protein NMR chemical shift calculations based on the automated fragmentation QM/MM approach. J Phys Chem B. 2009; 113:10380–10388. [PubMed: 19575540]

206. Karplus M. Molecular dynamics simulations of biomolecules. Acc Chem Res. 2002; 35:321–323. [PubMed: 12069615]

207. Mulder F, Filatov M. NMR chemical shift data and *ab initio* shielding calculations: emerging tools for protein structure determination. Chem Soc Rev. 2010; 39:578–590. [PubMed: 20111782]

208. Middleton, DA. Structural biology. In: Harris, RK.; Wasylishen, RE.; Duer, MJ., editors. NMR Crystallography. Wiley; 2009. p. 417-432.

209. Clearfield, A.; Reibenspies, JH.; Bhuvanesh, N. Principles and Applications of Powder Diffraction. Wiley; 2009.

210. Ando I, Kuroki S, Kurosu H, Yamanobe T. NMR chemical shift calculations and structural characterizations of polymers. Prog NMR Spectrosc. 2001; 39:79–133.

211. Ando I, Kurosu H, Uchida M, Yamanobe T. Modeling chemical shifts in polymers and amorphous matter. Abstr Papers Am Chem Soc. 1998; 216 (057-COMP).

212. Kuroki S, Nanba J, Ando I, Ogawa T, Murakami M. Solid state NMR investigation of the structures and dynamics of poly(silylenemethylene)s. Polym J. 1999; 31:369–374.

213. Kurosu H, Ando S, Yoshimizu H, Ando I. NMR studies of higher-order structures of solid polymers. Ann Rep NMR Spectrosc. 1994:189–321.

214. Satoh H, Kuroki S, Ando I. Structural changes of bulk polyethylene by stress impact as studied by solid-state NMR. J Appl Polym Sci. 2001; 82:2268–2272.

215. Ling Y, Zhang Y. Deciphering the NMR fingerprints of the disordered system with quantum chemical studies. J Phys Chem A. 2009; 113:5993–5997. [PubMed: 19331332]

216. Yannoni CS, Johnson RD, Meijer G, Bethune DS, Salem JR. Carbon-13 NMR study of the C_{60} cluster in the solid state: molecular motion and carbon chemical shift anisotropy. J Phys Chem. 1991; 95:9–10.

217. Orendt, AM. Fullerenes and related molecules as studied by solid state NMR. In: Grant, DM.; Harris, RK., editors. Encyclopedia of Nuclear Magnetic Resonance. Vol. 9. John Wiley & Sons; Chichester: 2002. p. 551-558.

218. Lai L, Lu J, Song W, Ni M, Wang L, Luo G, Zhou J, Mei WN, Gao Z, Yu D. First-principles calculation of ^{13}C NMR chemical shifts of infinite single-walled carbon nanotubes: new data for large-diameter and four-helical nanotubes. J Phys Chem C. 2008; 112:16417–16421.

219. Hu JZ, Solum MS, Taylor CMV, Pugmire RJ, Grant DM. Structural determination in carbonaceous solids using advanced solid state NMR techniques. Energy Fuels. 2001; 15:14–22.

220. Jiang YJ, Solum MS, Pugmire RJ, Grant DM, Schobert HH, Pappano PJ. New method for measuring the graphite content of anthracite coals and soots, Preprints of Symposia – Am. Chem. Soc. Div Fuel Chem. 2002; 47:629–631.

221. Van Niekerk D, Pugmire RJ, Solum MS, Painter PC, Mathews JP. Structural characterization of vitrinite-rich and inertinite-rich Permian-aged South African bituminous coals. Int J Coal Geol. 2008; 76:290–300.

222. Sethi NK, Pugmire RJ, Facelli JC, Grant DM. Quantitative determination of different carbon types in fusinite and anthracite coals from carbon-13 nuclear magnetic resonance chemical shielding line-shape analysis. Anal Chem. 2002; 60:1574–1579.

223. Elyashberg ME, Blinov KA, Williams AJ. The application of empirical methods of ^{13}C NMR chemical shift prediction as a filter for determining possible relative stereochemistry. Magn Reson Chem. 2009; 47:333–341. [PubMed: 19206140]

224. Bremser W. Hose – a novel substructure code. Anal Chim Acta. 1978; 103:355–365.

225. Harris, KDM.; Xu, M. Combined analysis of NMR & powder diffraction data. In: Harris, RK.; Wasylishen, RE.; Duer, MJ., editors. NMR Crystallography. Wiley; 2009. p. 275-286.

226. Meejoo S, Benson Kariuki M, Simon Kitchin J, Eugene Cheung Y, Albesa-Jové D, Kenneth Harris DM. Structural aspects of the β-polymorph of (E)-4-formylcinnamic acid: structure determination directly from powder diffraction data and elucidation of structural disorder from solid-state NMR. Helv Chim Acta. 2003; 86:1467–1477.

227. Witter R, Sternberg U, Hesse S, Kondo T, Koch F-T, Ulrich AS. ^{13}C chemical shift constrained crystal structure refinement of cellulose Ia and its verification by NMR anisotropy experiments. Macromolecules. 2006; 39:6125–6132.

228. Nishiyama Y, Sugiyama J, Chanzy H, Langan P. Crystal structure and hydrogen bonding system in cellulose 1(a), from synchrotron X-ray and neutron fiber diffraction. J Am Chem Soc. 2003; 125:14300–14306. [PubMed: 14624578]

229. Harper JK, Doebbler JA, Jacques E, Grant DM, Von Dreele RB. A combined solid-state NMR and synchrotron X-ray diffraction powder study on the structure of the antioxidant (+)-catechin 4.5-hydrate. J Am Chem Soc. 2010; 132:2928–2937. [PubMed: 20143807]

230. Harper JK, Facelli JC, Barich DH, McGeorge G, Mulgrew AE, Grant DM. ^{13}C NMR investigation of solid-state polymorphism in 10-deacetyl baccatin III. J Am Chem Soc. 2002; 124:10589–10595. [PubMed: 12197761]

231. Heider EM, Harper JK, Grant DM. Structural characterization of an anhydrous polymorph of paclitaxel by solid-state NMR. Phys Chem Chem Phys. 2007; 9:6083–6097. [PubMed: 18167583]

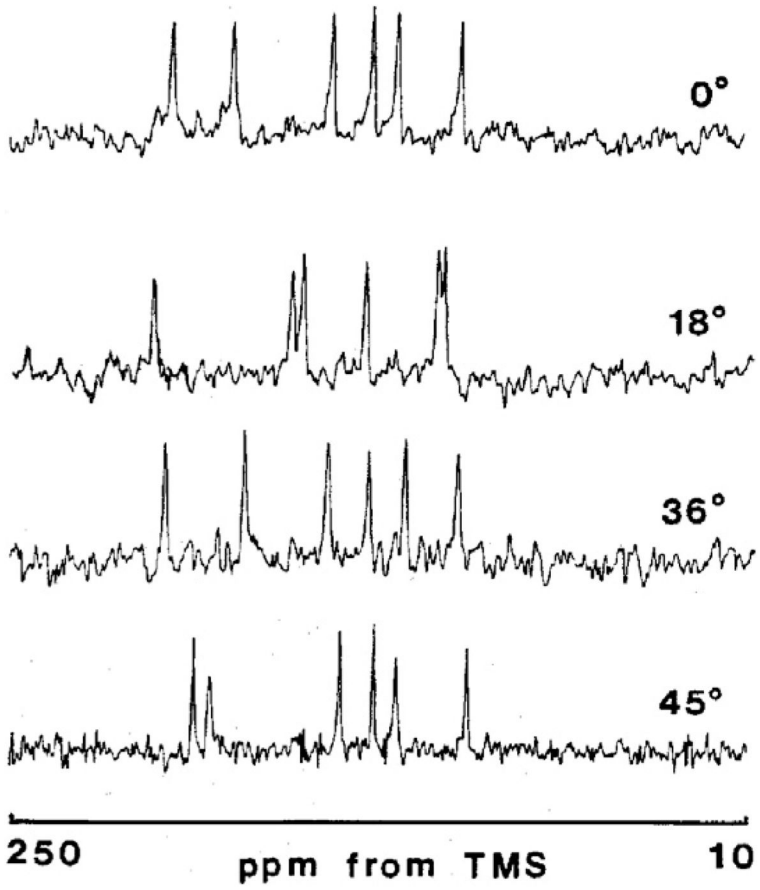

Fig. 1.

Representative 25.1 MHz ^{13}C NMR spectra of a single crystal of 1,3,5-trihydroxybenzene at different orientations with respect to the external magnetic field. From “Nuclear Magnetic Resonance Studies in Organic Single Crystals: Chemical Shift Anisotropy of Aromatic Molecules”, C.M. Carter, Ph.D. Thesis, The University of Utah, 1987.

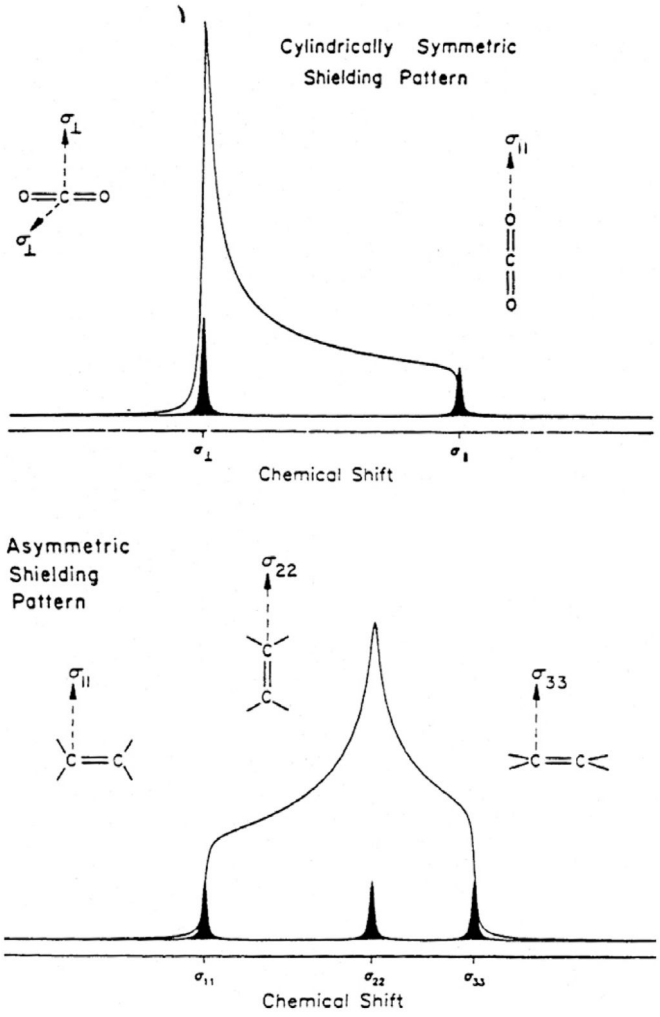

Fig. 2.
Powder pattern spectra for symmetric and asymmetric shielding tensors. From Ref. [23].

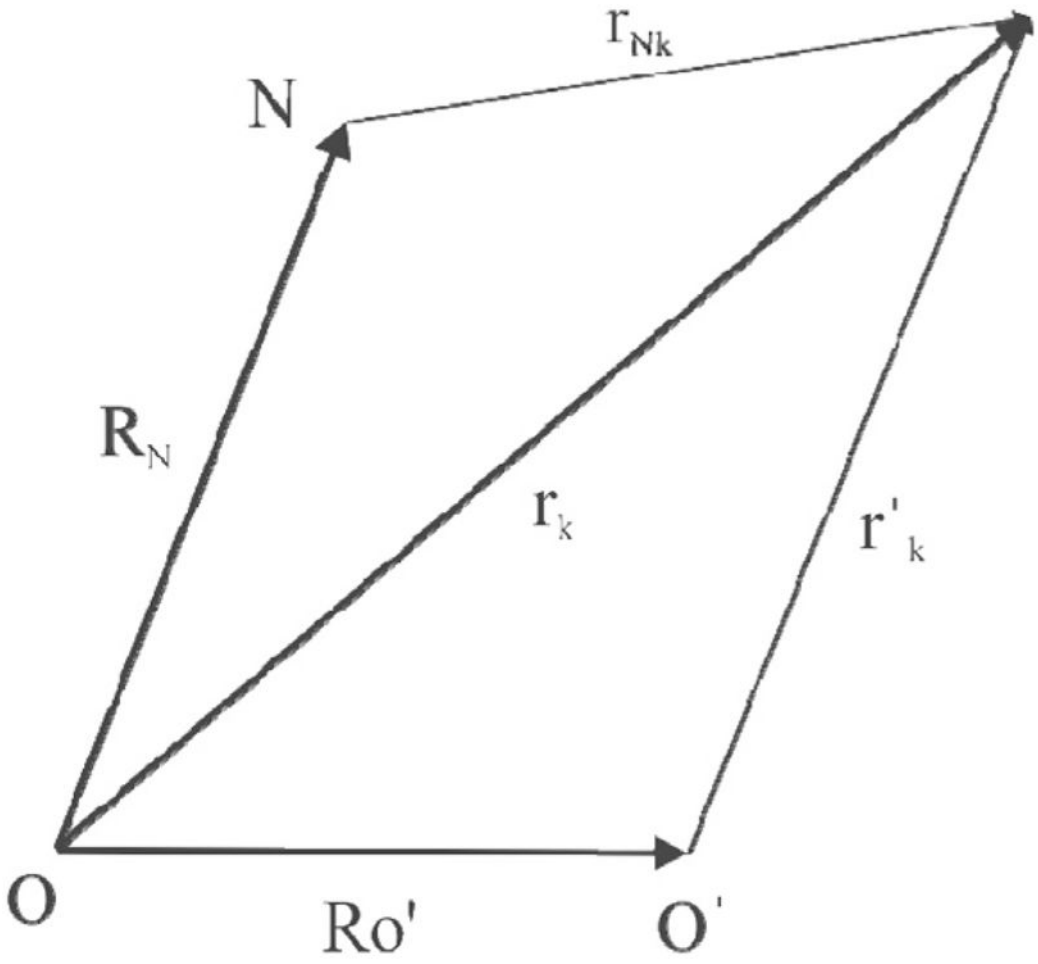

Fig. 3.

Coordinate system used to illustrate the gauge origin dependence of the diamagnetic and paramagnetic contributions of the shielding. **O** is the origin of coordinates, $\mathbf{O}'$ is the new origin of coordinates, $\mathbf{R}_{\mathbf{O}'}$ is the position of the new origin of coordinates with respect to original one, $\mathbf{R}_N$ is the position of the nucleus *N*, $\mathbf{r}_k$ is the position of the electron with respect to **O**, $\mathbf{r}_{Nk}$ is the position of the electron with respect to the nucleus *N* and $\mathbf{r}'_k$ is the position of the electron relative to the new origin of coordinates $\mathbf{O}'$.

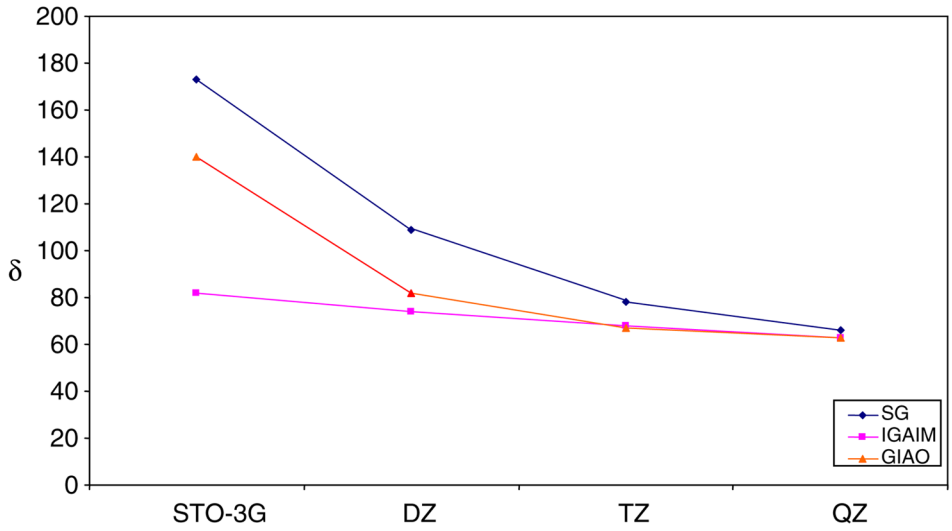

Fig. 4.

Basis set dependence of the $^{13}CH_2$ shieldings, δ, in glycine with different distributed gauge methods. SG: Single Gauge, IGAIM: Individual Gauge for Atoms in Molecules and GIAO: Gauge Including Atomic Orbitals. All the values are in ppm referenced to the bare nucleus. Calculations performed for the STO-3G, double zeta (DZ), triple zeta (TZ) and quadruple zeta (QZ) basis sets. From Ref. [135].

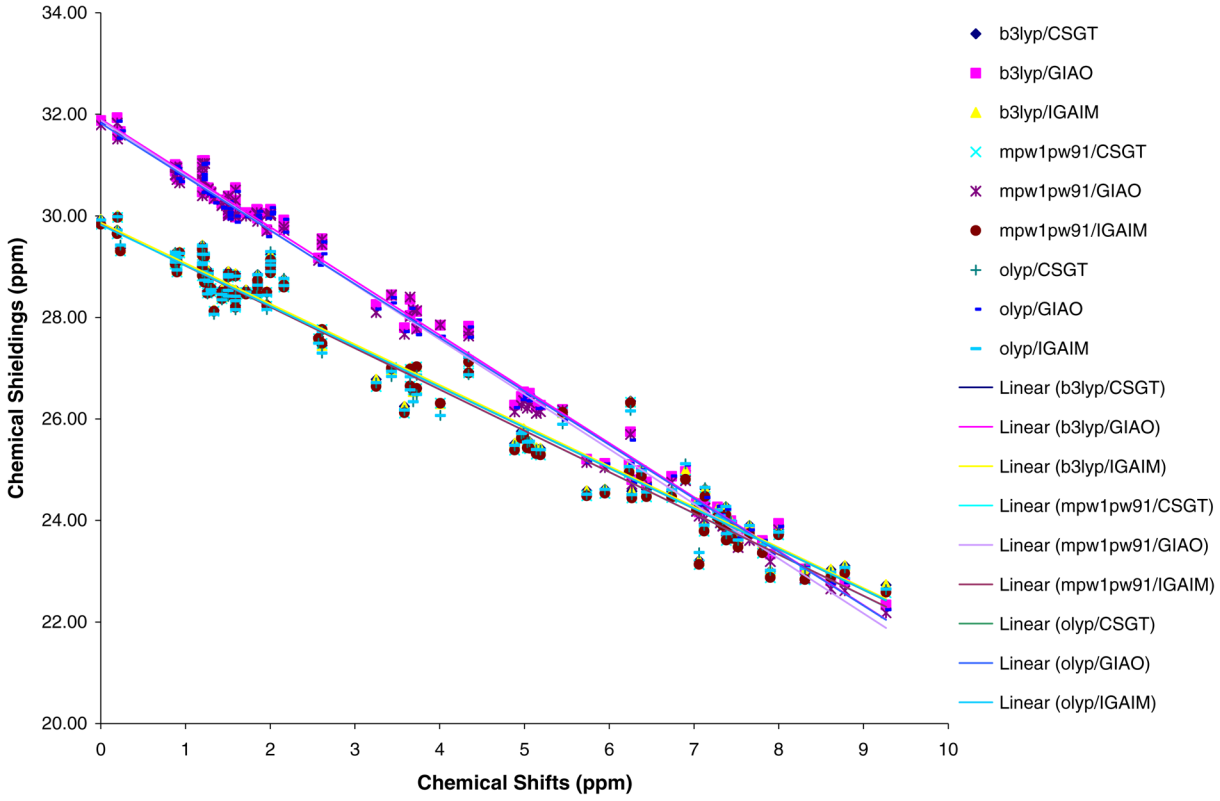

Fig. 5.

Calculated ^{1}H shieldings (vertical axis) vs. experimental chemical shifts (horizontal axis) for different exchange-correlation functionals with the GIAO, CSGT and IGAIM approaches for selected molecules in the G2 and G3 set of molecules. From Ref. [191].

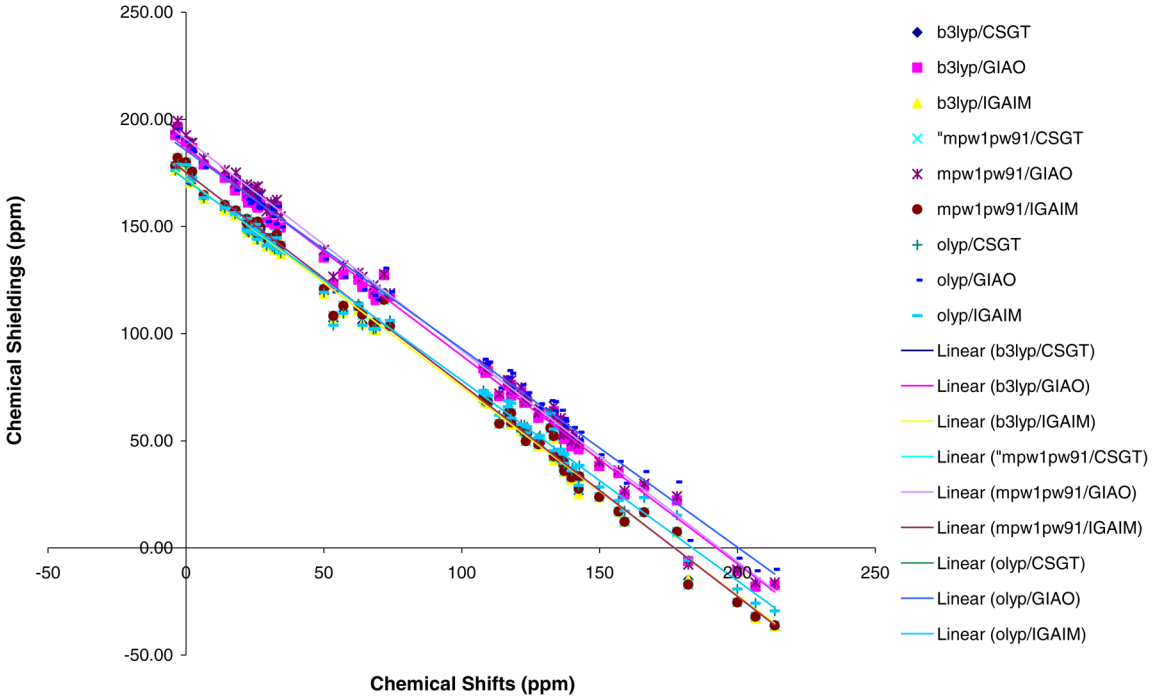

Fig. 6.

Calculated ^{13}C shieldings (vertical axis) vs. experimental chemical shifts (horizontal axis) for different exchange-correlation functionals with the GIAO, CSGT and IGAIM approaches for selected molecules in the G2 and G3 set of molecules. From Ref. [191].

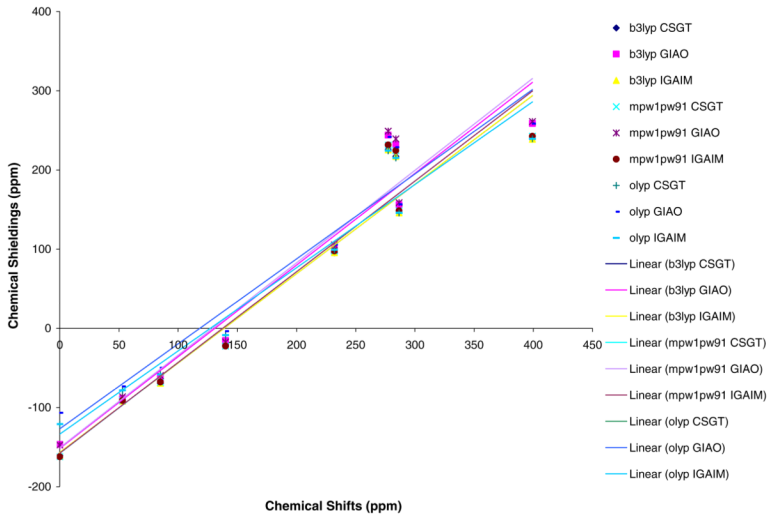

Fig. 7.

Calculated ^{15}N shieldings (vertical axis) vs. experimental chemical shifts (horizontal axis) for different exchange-correlation functionals with the GIAO, CSGT and IGAIM approaches for selected molecules in the G2 and G3 set of molecules. From Ref. [191].

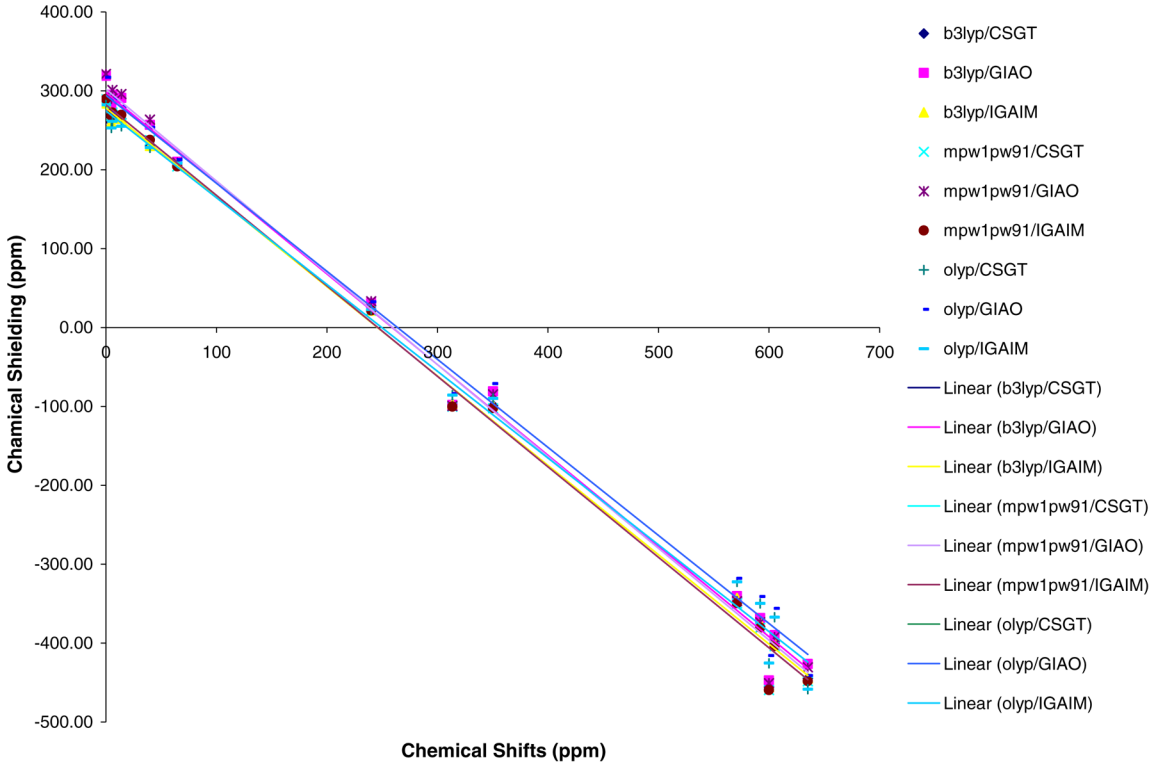

Fig. 8.

Calculated ^{17}O shieldings (vertical axis) vs. experimental chemical shifts (horizontal axis) for different exchange-correlation functionals with the GIAO, CSGT and IGAIM approaches for selected molecules in the G2 and G3 set of molecules. From Ref. [191].

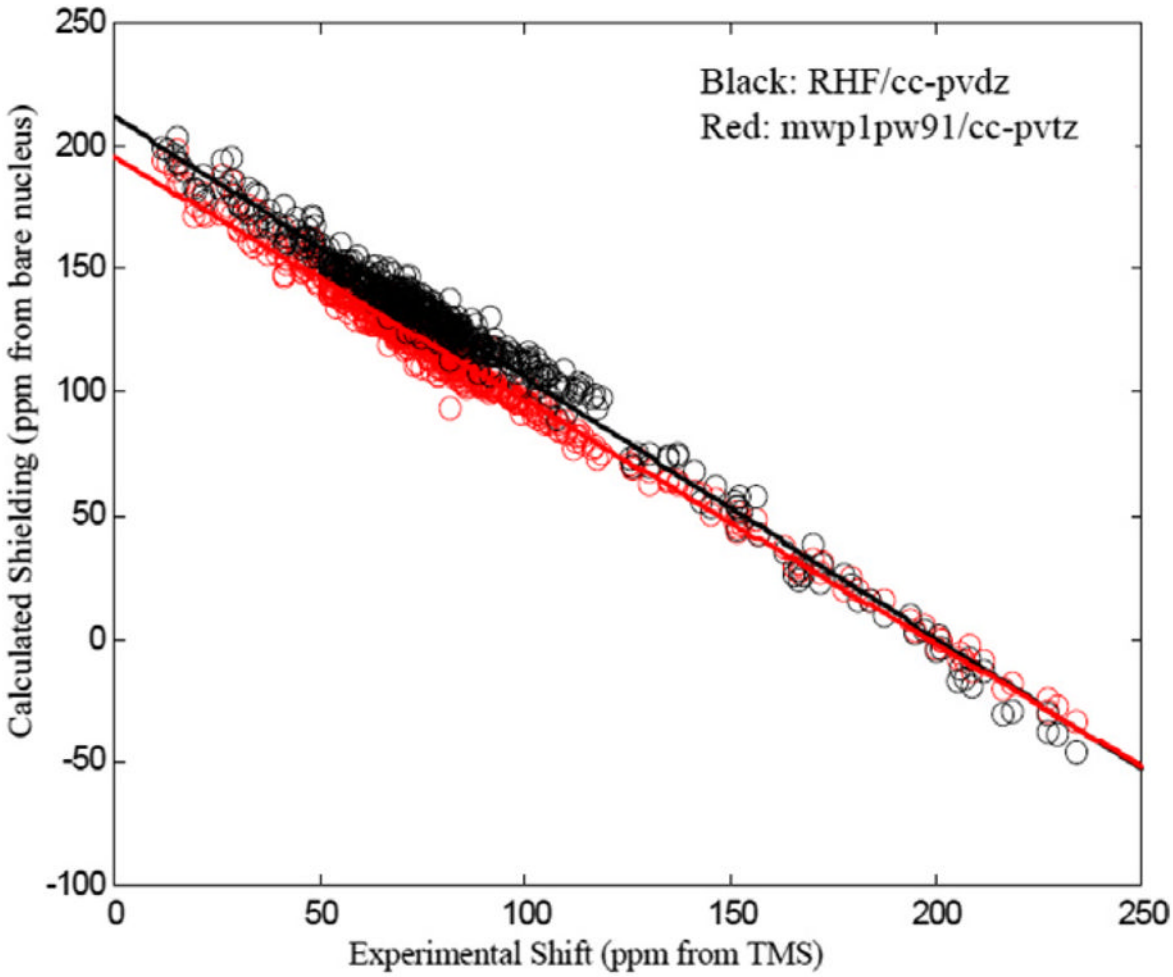

Fig. 9.

Linear correlation between calculated shielding and experimental shift tensor components. The lowest rmsd Hartree-Fock method, rhf/cc-pvdz, and DFT method, mwp1pw91/cc-pvtz, are plotted. The tensor parameters are in the icosahedral representation [194]. From Ref. [17].

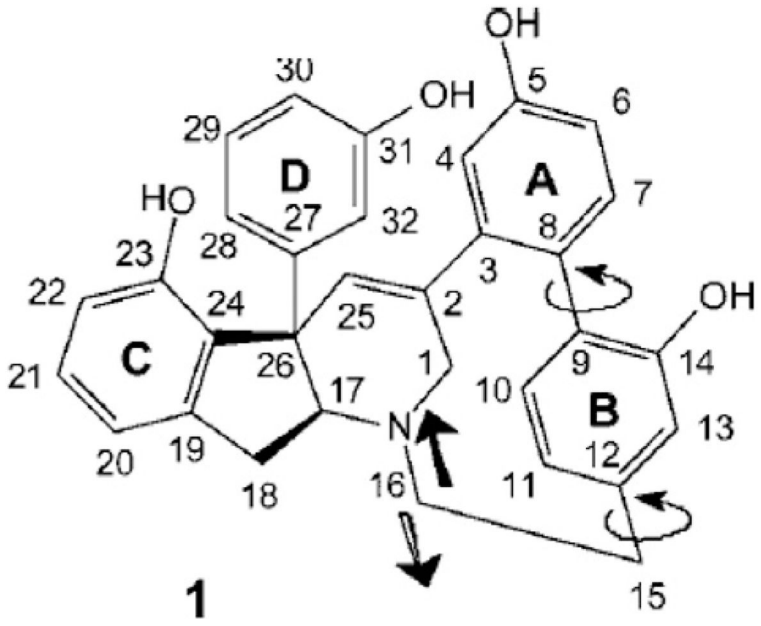

Fig. 10.
Haouamine A and the possible intermolecular motions that have been identified in this molecule (N-inversion and phenylene group rotation). Reproduced from Ref. [196].

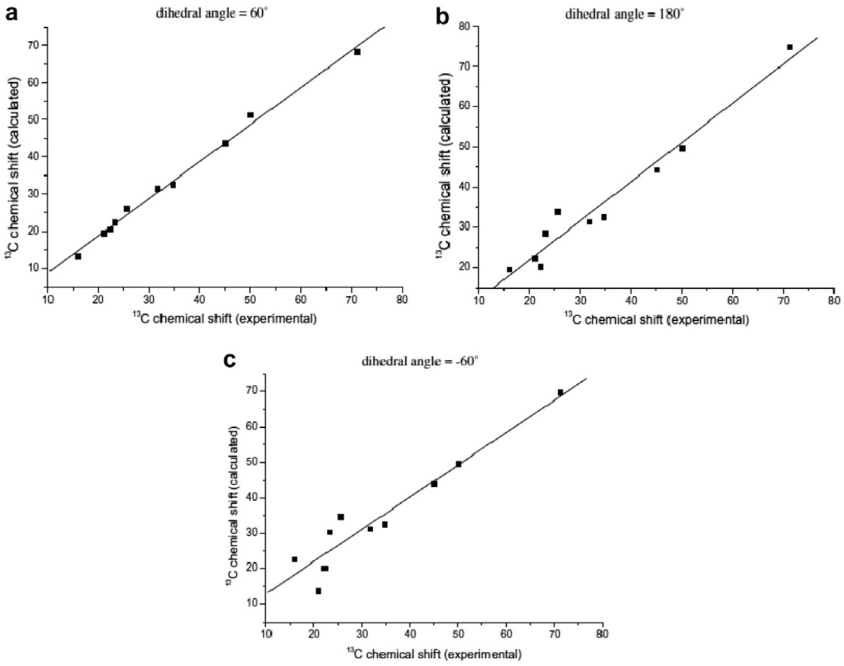

Fig. 11.

Fits between experimental and calculated ^{13}C chemical shifts for menthol conformers with different dihedral angles of the isopropyl group. Reproduced from Ref. [197].

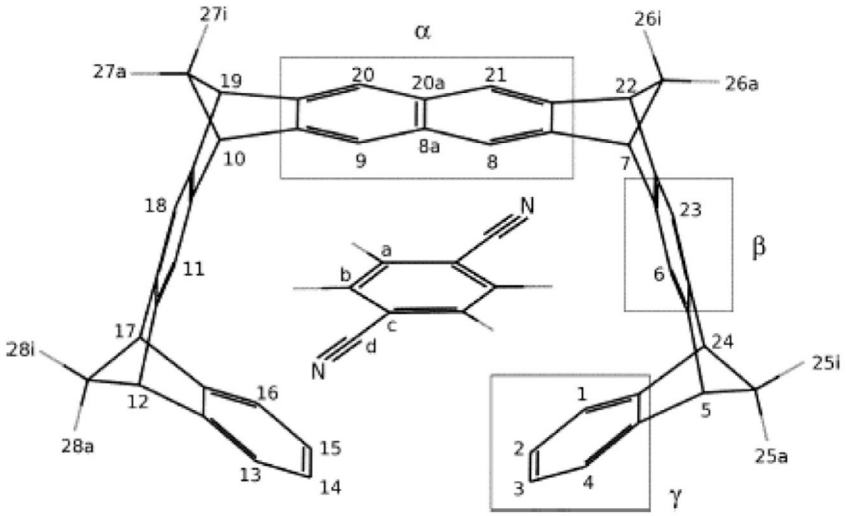

Fig. 12.
Schematic structure of the naphthalene molecular tweezers host guest complex with dicyanobenzene guest. From Ref. [199].

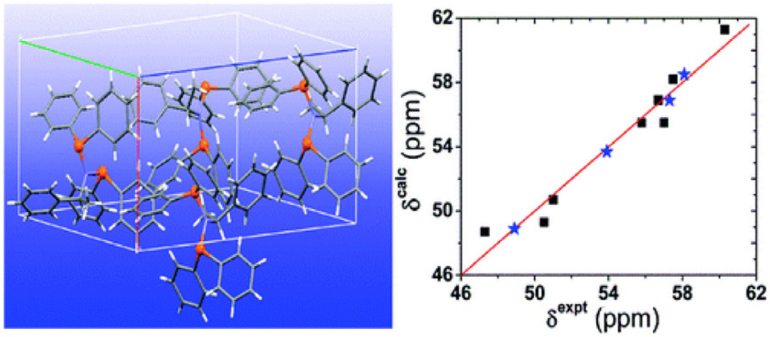

Fig. 13.

Unit cell of N,N-bis(diphenylphosphino)-N-((S)-α-methylbenzyl)amine and correlation between calculated and experimental ^{31}P chemical shifts in the same compound. There are two resonances for each molecule for a total of eight different resonances. The points marked as stars correspond to the average chemical shifts for each molecule in the unit cell. From Ref. [215].

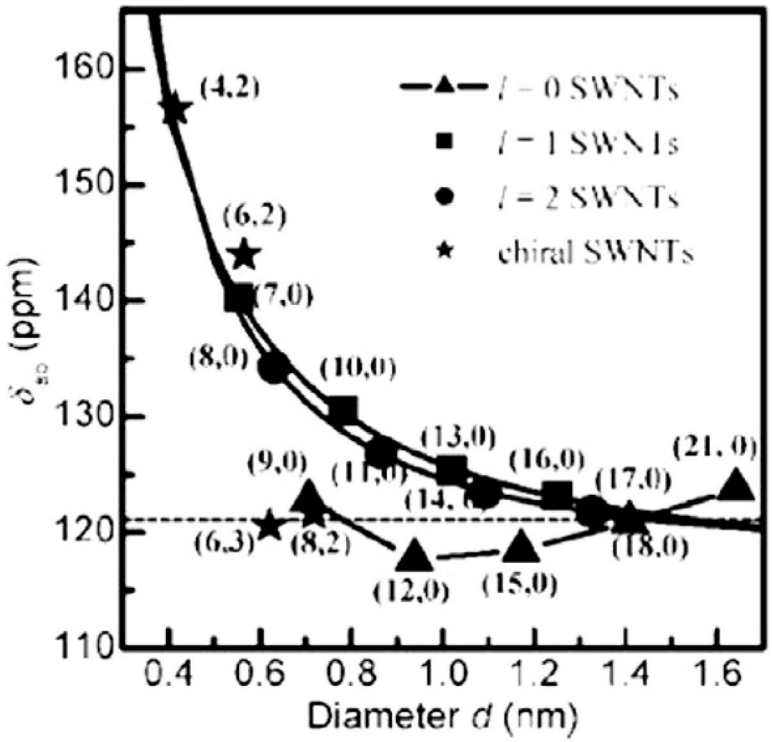

Fig. 14.

Calculated ^{13}C isotropic chemical shifts, δ_{iso}, of the zigzag (n) 7–21 and four chiral (4, 2), (6, 2), (6, 3), and (8, 2) single-walled nanotubes (SWNTs) as a function of the tube diameter (d). The solid black lines are the fits to $l = 1$ and 2 zigzag SWNTs, respectively. Where $l = \mathrm{mod}(n - m, 3)$. The calculated δ_{iso} of an isolated graphene sheet is labeled as a black dashed line. The values of the semimetallic SWNTs are averaged over the maximal neighboring odd and even Monkhorst-Pack k-points. From Ref. [218].

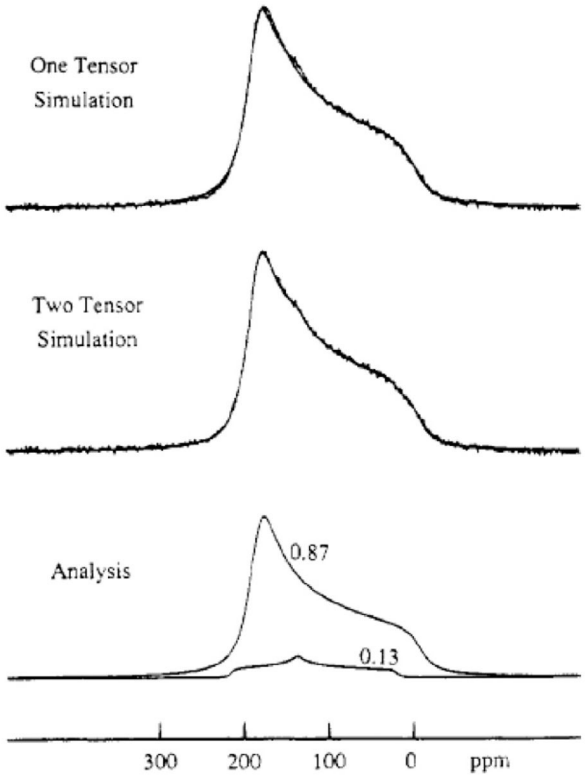

Fig. 15.

Experimental and simulated (overlaid) static spectra of the Pennsylvania anthracene coal number PSOC-867. The lower trace shows the bands and relative intensities used to obtain the two tensor fit. Reproduced from Ref. [222].

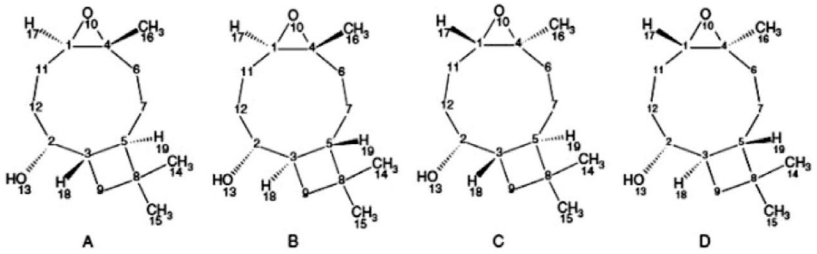

Fig. 16.
Stereoisomers of artarborol that are consistent with the calculated ^{1}H and ^{13}C chemical shifts. From Ref. [224].

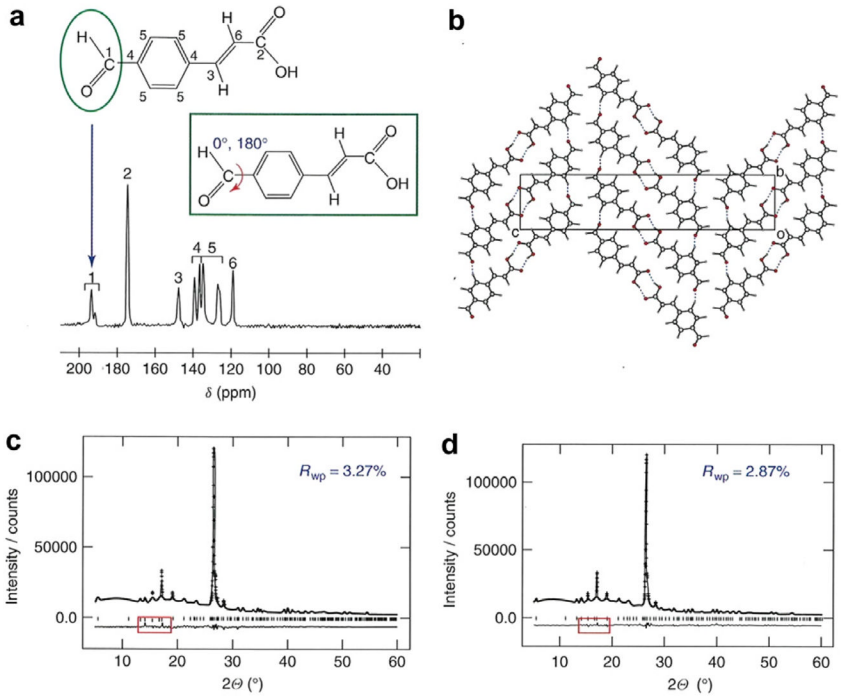

Fig. 17.

(a) High-resolution solid state NMR spectrum for the β-polymorph of the *p*-formyl-*trans*-cinnamic acid with the proposed disorder of the formyl group shown in the insert. (b) Crystal structure of the β-polymorph of *p*-formyl-*trans*-cinnamic acid determined from powder X-ray diffraction data viewed along the *a* axis and with only the major orientation of the formyl group shown. Powder-ray diffraction Rietveld refinement of the β-polymorph of *p*-formyl-*trans*-cinnamic acid is shown in (c) and (d) for the ordered model of the formyl group (R_{wp} = 3.27%) and the disordered model of the formyl group (R_{wp} = 2.87%), respectively. Apart from the description of the order/disorder of the formyl group, all other aspects of the refinement calculations are the same for (c) and (d). The red boxes highlight the region of the powder X-ray diffraction pattern corresponding to the greatest improvement in the quality of the fit of the disordered model. From Ref. [226].

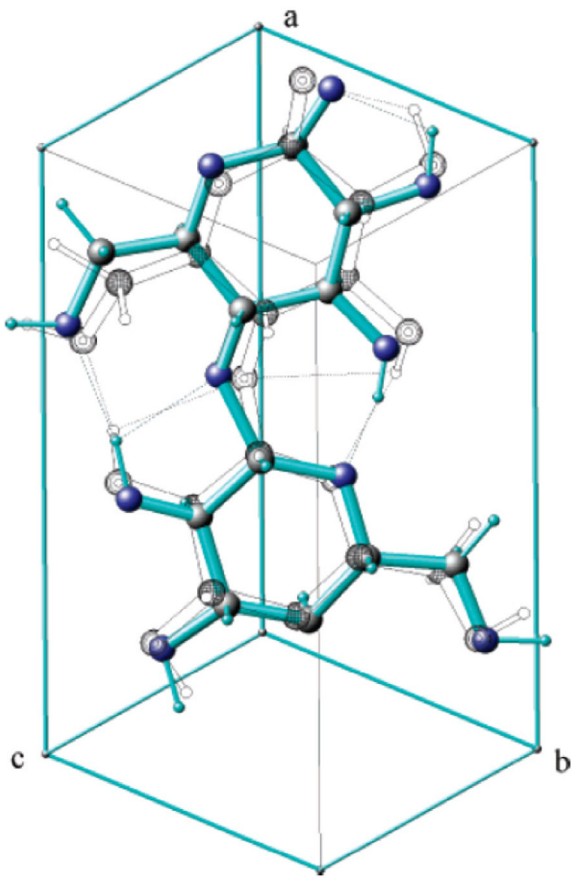

Fig. 18.

Least-squares superposition of the chemical shift optimized structure with the original neutron diffraction structure of Nishiyama et al. [228] (shown as the transparent model). The rms difference for all atoms is 0.57 Å and 0.37 Å for heavy atoms alone. The unit cell is viewed from slightly below the origin of *a*/*b*/*c*. From Ref. [227].

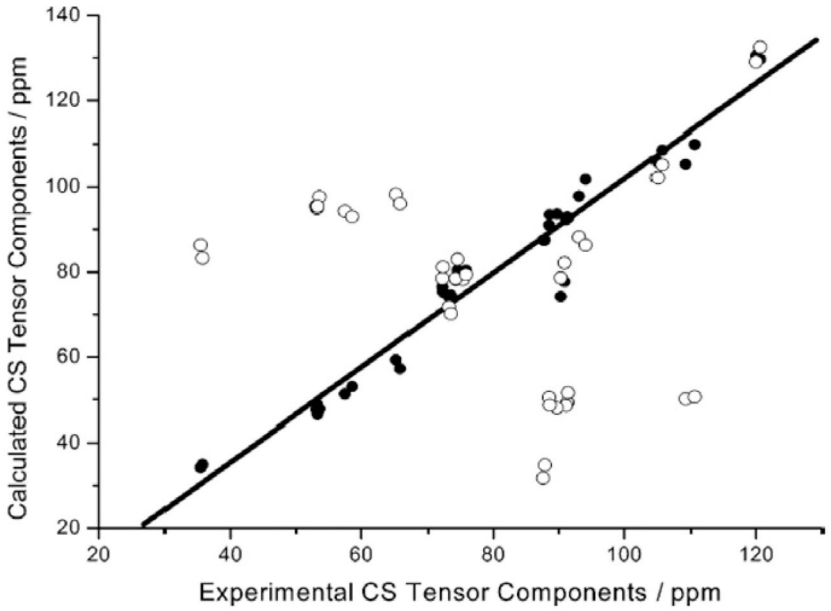

Fig. 19.

Calculated principal ^{13}C chemical shift tensor components (δ_{11}, δ_{22}, δ_{33}) plotted against the experimental values. The values after optimization with isotropic chemical shift-pseudo forces are displayed as filled circles (●), while the result evaluated from the original (non-optimized) diffraction structure are open circles (○). From Ref. [227].

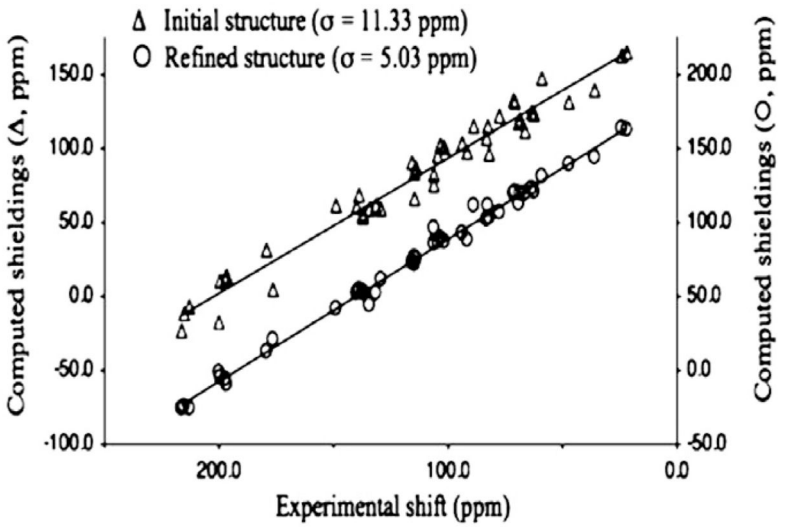

Fig. 20.

The initial structure, solved using XRD for the heavy-atom positions and SSNMR for the OH hydrogen orientations, is in excellent agreement with diffraction data but gives a poor fit of the computed ^{13}C shielding tensor principal values with the corresponding experimental data. This large error in the SSNMR fit indicated that further refinement was possible. A significant improvement in the fit (○) was obtained in the final refinement by adjusting bond lengths and valence angles computationally, while holding dihedral angles constant at XRD values. Computed shielding at sp^2 sites have systematic errors that are less problematic at sp^3 carbons. The trend lines shown here are intended to show only overall improvement in the correlation and do not reflect these systematic differences. From Ref. [229].

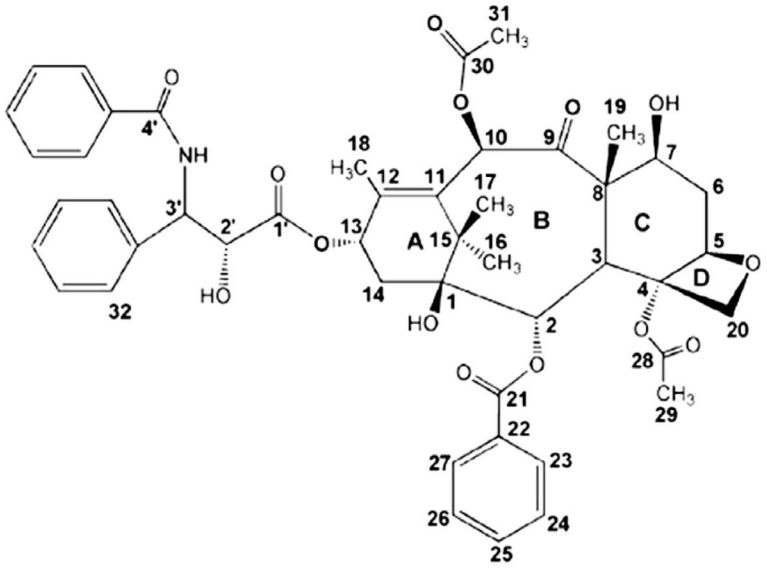

Fig. 21.
Atom numbering used in paclitaxel from Ref. [231].

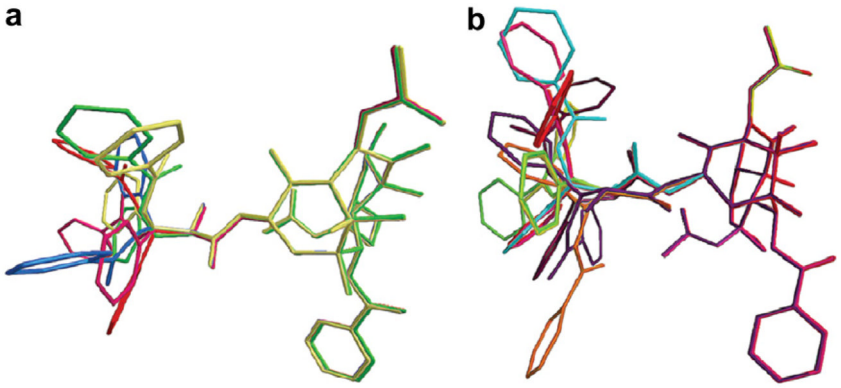

Fig. 22.
The five conformer models (a) providing high probability matches to the experimental chemical shift principal values of paclitaxel (form 2a) and the eight conformers (b) models providing probable matches to the experimental chemical shift principal values of paclitaxel (form 2b). From Ref. [231]

Table 1

Absolute shieldings (ppm) of commonly used reference compounds. All values are from Ref. [26].

Nucleus	Primary reference	Secondary reference
^{1}H	H atom, $\sigma_{iso} = 17.733$	H_2O, $\sigma_{iso} = 25.790$
^{13}C	CO, $\sigma_{iso} = 3.20$	TMS, $\sigma_{iso} = 185.4$
^{15}N	NH_3, $\sigma_{iso} = 264.54$	CH_3NO_2, $\sigma_{iso} = -135.0$
^{17}O	CO, $\sigma_{iso} = -42.3$	H_2O, $\sigma_{iso} = 307.9$
^{19}F	HF, $\sigma_{iso} = 410$	$CFCl_3$, $\sigma_{iso} = 189.9$
^{31}P	PH_3, $\sigma_{iso} = 597$	H_3PO_4, $\sigma_{iso} = 356$
^{33}S	OCS, $\sigma_{iso} = 843$	CS_2, $\sigma_{iso} = 581$

Table 2

Non-vanishing components of the diamagnetic, $\sigma^{d}_{\alpha\beta}$ and paramagnetic, $\sigma^{p}_{\alpha\beta}$, components of the shielding tensor for different point groups. From Ref. [30].

Point group symmetry at the site of the nucleus	Number of independent components		Non-vanishing components for the symmetric, $\sigma^{s}_{\alpha\beta}$ and antisymmetric, $\sigma^{a}_{\alpha\beta}$, components
	$\sigma^{s}_{\alpha\beta}$	$\sigma^{a}_{\alpha\beta}$	
C_1, C_i	6	9	σ_{zz}, σ_{xx}, σ_{yy}, σ^{s}_{xy}, σ^{s}_{xz}, σ^{s}_{yz};σ^{a}_{xy}, σ^{a}_{xz}, σ^{a}_{yz}
C_2, C_s, C_{2h}	4	5	σ_{zz}, σ_{xx}, σ_{yy}, σ^{s}_{xy};σ^{a}_{xy}
C_{2v}, D_2, D_{2h}	3	3	σ_{zz}, σ_{xx}, σ_{yy}
C_4, S_4, C_{4h}	2	3	σ_{zz}, σ_{xx}, σ_{yy}; σ^{a}_{xy}
C_3, S_6, C_{3h}, C_6, C_{6h}	2	3	σ_{zz}, $\sigma_{xx} = \sigma_{yy}$; σ^{a}_{xy}
C_{4v}, D_{2d}, D_4, D_{4h}, C_{3v}, D_3, D_{3d}, D_{3h}, D_{4h}, D_{3h}, C_{6v}, D_6, D_{6h}	2	2	σ_{zz}, $\sigma_{xx} = \sigma_{yy}$
$C_{\infty v}$, $D_{\infty h}$	2	1	σ_{zz}, $\sigma_{xx}=\sigma_{yy}(\sigma^{p}_{zz}=0)_a$
T, T_h, T_d, O, O_h	1	1	$\sigma_{zz} = \sigma_{xx} = \sigma_{yy}$

[a]Paramagnetic component along the *z*-axes.

Table 3

Calculated effects of the electron correlation on chemical shifts using different methods. All values are absolute shieldings in ppm, from Ref. [110].

	SCF	MP2	MP3	MP4	CCSD	CCSD(T)	MCSF	Exp.
CH_4: ^{13}C	194.8	201.0	198.8	199.5	198.7	199.1	198.2	198.4
CO: ^{13}C	−25.5	10.6	−4.2	12.7	0.8	5.6	8.2	3.29
CO: ^{17}O	−87.7	−46.5	−68.3	−44.0	−56.0	−52.9	−38.9	−38.7
H_2O: ^{17}O	328.1	346.1	336.7	339.7	336.9	337.9	335.3	357.6
NH_3: ^{15}N	262.3	276.5	270.1	271.8	269.7	270.7		273.3
N_2: ^{15}N	−112.4	−41.6	−72.2	−48.5	−53.9	−58.1	−53.1	−57.3
HF: ^{19}F	413.6	424.2	417.8	419.9	418.1	418.6	419.6	420.0
F_2: ^{19}F	−167.9	−170.0	−176.9	−180.7	−171.1	−186.5	−136.6	−196.0

Prog Nucl Magn Reson Spectrosc. Author manuscript; available in PMC 2012 May 01.

Table 4

RMS error between calculated and experimental chemical shifts for different exchange correlation functional for a set of small molecules. All values are in ppm from Refs. [115,116], calculated using the GIAO method with a qz2p basis set and MP2/tz2p geometries.

RMS	HF	LDA	BPW91	BLYP	B3PW91	B3LYP	MP2
^{13}C	11.5	16.1	7.7	9.2	8.7	9.5	2.3
^{15}N	49.3	34.6	20.0	21.7	27.5	29.1	13.4

Table 5

Standard deviation, Stdv., the slope and the intercept defining the linear correlation between calculated ^{1}H shieldings and measured chemical shifts in selected molecules from the G2 and G3 sets. From Ref. [191].

	B3LYP			MPW1PW91			OLYP		
	CSGT	GIAO	IGAIM	CSGT	GIAO	IGAIM	CSGT	GIAO	IGAIM
Stdv.	0.341	0.195	0.340	0.342	0.203	0.341	0.353	0.201	0.352
Slope	−1.21	−0.93	−1.21	−1.21	−1.21	−1.21	−1.21	−1.21	−1.21
Intercept	36.4	29.8	29.8	29.8	29.8	29.8	29.8	29.8	29.8

Prog Nucl Magn Reson Spectrosc. Author manuscript; available in PMC 2012 May 01.

Table 6

Standard deviation, Stdv., the slope and the intercept defining the linear correlation between calculated ^{13}C shieldings and measured chemical shifts in selected molecules from the G2 and G3 sets. From Ref. [191].

	B3LYP			MPW1PW91			OLYP		
	CSGT	GIAO	IGAIM	CSGT	GIAO	IGAIM	CSGT	GIAO	IGAIM
Stdv.	4.1056	3.6650	4.109	3.780	3.385	3.782	4.595	4.1226	4.5994
Slope	−1.02	−1.02	−1.02	−1.02	−1.02	−1.02	−1.02	−1.02	−1.02
Intercept	176.7	191.9	191.9	191.9	191.9	191.9	191.9	191.9	191.9

Prog Nucl Magn Reson Spectrosc. Author manuscript; available in PMC 2012 May 01.

Table 7

Standard deviation, Stdv., the slope and the intercept defining the linear correlation between calculated ^{15}N shieldings and measured chemical shifts in selected molecules from the G2 and G3 sets. From Ref. [191].

	B3LYP			MPW1PW91			OLYP		
	CSGT	**GIAO**	**IGAIM**	**CSGT**	**GIAO**	**IGAIM**	**CSGT**	**GIAO**	**IGAIM**
Stdv.	38.40	40.16	38.40	40.32	41.83	40.32	36.66	38.48	36.65
Slope	0.83	0.81	0.81	0.81	0.81	0.81	0.81	0.81	0.81
Intercept	141.4	134.1	134.1	134.1	134.1	134.1	134.1	134.1	134.1

Prog Nucl Magn Reson Spectrosc. Author manuscript; available in PMC 2012 May 01.

Table 8

Standard deviation, Stdv., the slope and the intercept defining the linear correlation between calculated ^{15}N shieldings and measured chemical shifts in selected molecules from the G2 and G3 sets. From Ref. [191].

	B3LYP			MPW1PW91			OLYP		
	CSGT	GIAO	IGAIM	CSGT	GIAO	IGAIM	CSGT	GIAO	IGAIM
Stdv.	91.72	90.37	91.72	92.25	91.41	92.25	89.58	88.06	89.58
Slope	−0.96	−0.94	−0.94	−0.94	−0.94	−0.94	−0.94	−0.94	−0.94
Intercept	219.7	237.7	237.7	237.7	237.7	237.7	237.7	237.7	237.7